

Supporting Information: Near-linear scaling explicitly correlated coupled cluster method based on an open-shell domain-based local pair natural orbitals

Ashutosh Kumar and Edward F. Valeev*

*Department of Chemistry, Virginia Tech,
Blacksburg, Virginia 24061, United States*

Frank Neese

*Max-Planck-Institut für Chemische Energiekonversion,
Stiftstr. 34-36, D-45470 Mülheim an der Ruhr, Germany*

(Dated: August 10, 2020)

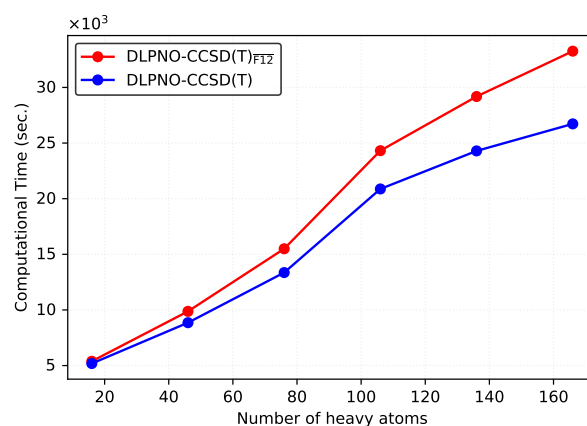


FIG. 1: Wall clock time in seconds for UHF-DLPNO-CCSD(T) and UHF-DLPNO-CCSD(T)_{FT2} correlation energy calculations with TightPNO settings for a series of triplet $[(C_4SH_3) - (CH_2)_N - (C_4SH_3)^{2+}]$ diradical molecules from $N=0$ to $N=50$. Following basis set quartet were used: {def2-TZVP, def2-TZVP/RI, cc-pVDZ-F12-OptRI, def2/J} {OBS, DFBS, CABS, CDFBS} and the COSX procedure for evaluating the exchange operator was employed. All these calculations utilized 4 CPU cores (4 MPI processes) and a total of 512 GB memory.

TABLE I: Comparison of heats of formation in kcal/mol calculated using the T0 and T1 approximations of the DLPNO-CCSD(T)_{F12} method with TightPNO settings for cc-pVDZ-F12 and cc-pVTZ-F12 basis set with the CBS extrapolated canonical CCSD(T) values. Errors with respect to the CBS results are shown in the parenthesis.

	cc-pVDZ-F12 ^a				cc-pVTZ-F12 ^b				CBS ^c
	T ₀		T ₁		T ₀		T ₁		
CH3CHOO	35.15	(2.13)	34.24	(-1.22)	35.17	(-2.15)	34.29	(-1.27)	33.02
CH2CHOOH	14.32	(-0.59)	13.82	(-0.09)	14.70	(-0.97)	14.20	(-0.47)	13.73
CH3CH2OO	14.13	(-0.02)	13.87	(0.24)	14.55	(-0.44)	14.31	(-0.20)	14.11
OHCH2CH2O	-20.14	(0.11)	-20.27	(0.24)	-19.87	(-0.16)	-19.99	(-0.04)	-20.03
OHCH2OCH2	-24.15	(-0.61)	-24.34	(-0.42)	-24.18	(-0.58)	-24.36	(-0.40)	-24.76
CH3OCH2O	-15.89	(0.03)	-16.05	(0.19)	-15.48	(-0.38)	-15.63	(-0.23)	-15.86
OHCHCH2OH	-31.38	(-0.70)	-31.56	(-0.52)	-31.58	(-0.50)	-31.75	(-0.33)	-32.08
(CH3)3C	34.95	(-0.35)	34.85	(-0.25)	34.73	(-0.13)	34.63	(-0.03)	34.60
CH3CH2CHCH3	38.49	(-0.35)	38.40	(-0.26)	38.31	(-0.17)	38.22	(-0.08)	38.14
CH3CH2CHOH	2.52	(-0.53)	2.38	(-0.39)	2.32	(-0.33)	2.19	(-0.20)	1.99
CH2CCCCH	190.24	(0.47)	189.35	(1.36)	191.18	(-0.47)	190.29	(0.42)	190.71
CHCCHCCH	192.04	(0.45)	191.22	(1.27)	192.93	(-0.44)	192.12	(0.37)	192.49
CH3OOO	26.56	(-0.02)	25.31	(1.23)	28.18	(-1.64)	26.97	(-0.43)	26.54
OCH2OOH	-2.32	(0.37)	-2.56	(0.61)	-1.50	(-0.45)	-1.72	(-0.23)	-1.95
OHCH2OO	-21.80	(0.11)	-22.09	(0.40)	-21.18	(-0.51)	-21.45	(-0.24)	-21.69
C(OH)3	-79.77	(-0.64)	-79.97	(-0.44)	-79.81	(-0.60)	-80.01	(-0.40)	-80.41
(CH3)2CHCH2	40.04	(-0.39)	39.93	(-0.28)	39.82	(-0.17)	39.71	(-0.06)	39.65
CH3CH(OH)CH2	6.26	(-0.50)	6.13	(-0.37)	6.09	(-0.33)	5.96	(-0.20)	5.76
CH3OCHOH	-25.29	(-0.59)	-25.48	(-0.40)	-25.27	(-0.61)	-25.46	(-0.42)	-25.88
CH2CH2CH2OH	8.77	(-0.45)	8.65	(-0.33)	8.63	(-0.31)	8.51	(-0.19)	8.32
CH3N(O)OH	13.77	(-0.45)	13.36	(-0.04)	14.16	(-0.84)	13.77	(-0.45)	13.32
CH3CHCH2OH	6.77	(-0.41)	6.65	(-0.29)	6.66	(-0.30)	6.55	(-0.19)	6.36
CHCCCO	144.04	(0.46)	142.85	(1.65)	145.45	(-0.95)	144.28	(0.22)	144.50
CH2CH2OOH	33.13	(-0.30)	32.90	(-0.07)	33.37	(-0.54)	33.16	(-0.33)	32.83
CH2CH2OCH3	19.95	(-0.49)	19.81	(-0.35)	19.88	(-0.42)	19.74	(-0.28)	19.46
CH3C(OH)CH3	-2.38	(-0.52)	-2.53	(-0.37)	-2.60	(-0.30)	-2.74	(-0.16)	-2.90
CH3CH2OCH2	13.33	(-0.73)	13.17	(-0.57)	13.09	(-0.49)	12.93	(-0.33)	12.60
CH3CH(O)CH3	9.81	(0.08)	9.70	(0.19)	9.96	(-0.07)	9.85	(0.04)	9.89
CH3CH2CH2O	12.48	(0.17)	12.37	(0.28)	12.69	(-0.04)	12.60	(0.05)	12.65
CH3CHOCH3	11.59	(-0.62)	11.43	(-0.46)	11.43	(-0.46)	11.27	(-0.30)	10.97
CHCCCOH	126.92	(-0.48)	125.86	(0.58)	127.54	(-1.10)	126.48	(-0.04)	126.44
CH2CCCO	103.73	(-0.72)	101.92	(1.09)	104.99	(-1.98)	103.19	(-0.18)	103.01
CH(OH)3	-129.63	(-0.98)	-129.85	(-0.76)	-129.88	(-0.73)	-130.10	(-0.51)	-130.61
OHCH2OOH	-60.21	(-0.80)	-60.52	(-0.49)	-60.13	(-0.88)	-60.43	(-0.58)	-61.01
OHOOH	5.95	(-0.48)	5.35	(0.12)	7.01	(-1.54)	6.42	(-0.95)	5.47
3c-CHCHCHCHC	172.90	(-0.40)	172.19	(0.31)	173.53	(-1.03)	172.83	(-0.33)	172.50
CH2CCCCH2	158.54	(-0.65)	157.06	(0.83)	159.63	(-1.74)	158.13	(-0.24)	157.89
CHCCH2CCH	158.87	(-0.20)	158.03	(0.64)	159.56	(-0.89)	158.71	(-0.04)	158.67
CH3CCCCH	149.13	(-0.50)	148.12	(0.51)	149.69	(-1.06)	148.67	(-0.04)	148.63
OCCHCH	98.64	(-0.17)	97.52	(0.95)	99.71	(-1.24)	98.59	(-0.12)	98.47
CH3CH2OOH	-21.64	(-0.81)	-21.92	(-0.53)	-21.68	(-0.77)	-21.95	(-0.50)	-22.45
CH3CH2CH2CH3	-12.74	(-0.83)	-12.89	(-0.68)	-13.17	(-0.40)	-13.31	(-0.26)	-13.57
(CH3)2CHCH3	-14.16	(-0.86)	-14.31	(-0.71)	-14.63	(-0.39)	-14.79	(-0.23)	-15.02
CH3OOCCH3	-12.07	(-0.83)	-12.37	(-0.53)	-11.98	(-0.92)	-12.29	(-0.61)	-12.90
OCOCO	25.57	(-0.27)	24.06	(1.24)	26.78	(-1.48)	25.29	(0.01)	25.30
CH3CH2OCH3	-35.56	(-0.92)	-35.74	(-0.74)	-35.84	(-0.64)	-36.03	(-0.45)	-36.48
CH2CCHCCH	155.00	(-0.31)	154.01	(0.68)	155.81	(-1.12)	154.80	(-0.11)	154.69
c-CHCHCHCHNH	68.51	(-1.41)	67.70	(-0.60)	68.57	(-1.47)	67.75	(-0.65)	67.10
CHCCCCCH	233.28	(-0.59)	231.67	(1.02)	234.29	(-1.60)	232.66	(0.03)	232.69
CHCCCCN	212.62	(0.45)	210.96	(2.11)	214.45	(-1.38)	212.78	(0.29)	213.07
Max		(-2.13)		(2.11)		(-2.15)		(-1.27)	
RMSD		(0.63)		(0.73)		(0.92)		(0.38)	

^a {cc-pVDZ-F12, cc-pVDZ-F12-OptRI, aug-cc-pVDZ/RI}

^b {cc-pVTZ-F12, cc-pVTZ-F12-OptRI, aug-cc-pVTZ/RI}

^c {a'5Z/a'QZ extrapolation}

TABLE II: Comparison of heats of formation in kcal/mol calculated using the T0 and T1 approximations of the DLPNO-CCSD(T)_{F12} method with TightPNO settings for aug-cc-pVDZ and aug-cc-pVTZ basis with the CBS extrapolated canonical CCSD(T) values. Errors with respect to the CBS results are shown in the parenthesis.

	aug-cc-pVDZ ^a				aug-cc-pVTZ ^b				CBS ^c
	T ₀		T ₁		T ₀		T ₁		
CH3CHOO	35.17	(-2.15)	34.26	(-1.24)	34.83	(-1.81)	33.94	(-0.92)	33.02
CH2CHOOH	14.18	(-0.45)	13.68	(0.05)	14.48	(-0.75)	13.98	(-0.25)	13.73
CH3CH2OO	13.33	(0.78)	13.08	(1.03)	14.02	(0.09)	13.77	(0.34)	14.11
OHCH2CH2O	-20.70	(0.67)	-20.83	(0.80)	-20.13	(0.10)	-20.24	(0.21)	-20.03
OHCH2OCH2	-24.76	(0.00)	-24.95	(0.19)	-24.40	(-0.36)	-24.59	(-0.17)	-24.76
CH3OCH2O	-16.59	(0.73)	-16.75	(0.89)	-15.87	(0.01)	-16.02	(0.16)	-15.86
OHCHCH2OH	-31.98	(-0.10)	-32.15	(0.07)	-31.71	(-0.37)	-31.87	(-0.21)	-32.08
(CH3)3C	34.61	(-0.01)	34.49	(0.11)	34.89	(-0.29)	34.79	(-0.19)	34.60
CH3CH2CHCH3	38.17	(-0.03)	38.06	(0.08)	38.44	(-0.30)	38.35	(-0.21)	38.14
CH3CH2CHOH	2.10	(-0.11)	1.96	(0.03)	2.32	(-0.33)	2.18	(-0.19)	1.99
CH2CCCCH	193.39	(-2.68)	192.47	(-1.76)	191.94	(-1.23)	191.04	(-0.33)	190.71
CHCCHCCH	195.10	(-2.61)	194.26	(-1.77)	193.72	(-1.23)	192.90	(-0.41)	192.49
CH3OOO	25.28	(1.26)	24.00	(2.54)	27.29	(-0.75)	26.07	(0.47)	26.54
OCH2OOH	-3.04	(1.09)	-3.28	(1.33)	-2.07	(0.12)	-2.29	(0.34)	-1.95
OHCH2OO	-22.67	(0.98)	-22.96	(1.27)	-21.83	(0.14)	-22.11	(0.42)	-21.69
C(OH)3	-80.47	(0.06)	-80.67	(0.26)	-80.10	(-0.31)	-80.29	(-0.12)	-80.41
(CH3)2CHCH2	39.55	(0.10)	39.43	(0.22)	39.95	(-0.30)	39.84	(-0.19)	39.65
CH3CH(OH)CH2	5.72	(0.04)	5.58	(0.18)	6.10	(-0.34)	5.97	(-0.21)	5.76
CH3OCHOH	-25.84	(-0.04)	-26.03	(0.15)	-25.53	(-0.35)	-25.72	(-0.16)	-25.88
CH2CH2CH2OH	8.27	(0.05)	8.15	(0.17)	8.64	(-0.32)	8.52	(-0.20)	8.32
CH3N(O)OH	13.17	(0.15)	12.77	(0.55)	13.63	(-0.31)	13.24	(0.08)	13.32
CH3CHCH2OH	6.40	(-0.04)	6.27	(0.09)	6.69	(-0.33)	6.57	(-0.21)	6.36
CHCCCO	146.68	(-2.18)	145.47	(-0.97)	146.04	(-1.54)	144.86	(-0.36)	144.50
CH2CH2OOH	32.53	(0.30)	32.31	(0.52)	33.16	(-0.33)	32.94	(-0.11)	32.83
CH2CH2OCH3	19.43	(0.03)	19.28	(0.18)	19.80	(-0.34)	19.66	(-0.20)	19.46
CH3C(OH)CH3	-2.74	(-0.16)	-2.89	(-0.01)	-2.59	(-0.31)	-2.73	(-0.17)	-2.90
CH3CH2OCH2	12.68	(-0.08)	12.51	(0.09)	12.96	(-0.36)	12.80	(-0.20)	12.60
CH3CH(O)CH3	9.29	(0.60)	9.17	(0.72)	9.88	(0.01)	9.77	(0.12)	9.89
CH3CH2CH2O	11.98	(0.67)	11.87	(0.78)	12.57	(0.08)	12.47	(0.18)	12.65
CH3CHOCH3	11.28	(-0.31)	11.12	(-0.15)	11.36	(-0.39)	11.20	(-0.23)	10.97
CHCCCOH	129.46	(-3.02)	128.39	(-1.95)	128.14	(-1.70)	127.07	(-0.63)	126.44
CH2CCCO	105.78	(-2.77)	103.95	(-0.94)	105.33	(-2.32)	103.52	(-0.51)	103.01
CH(OH)3	-130.66	(0.05)	-130.87	(0.26)	-130.27	(-0.34)	-130.49	(-0.12)	-130.61
OHCH2OOH	-61.28	(0.27)	-61.58	(0.57)	-60.65	(-0.36)	-60.96	(-0.05)	-61.01
OHOOH	4.77	(0.70)	4.18	(1.29)	6.14	(-0.67)	5.55	(-0.08)	5.47
3c-CHCHCHCHC	174.11	(-1.61)	173.39	(-0.89)	174.05	(-1.55)	173.34	(-0.84)	172.50
CH2CCCCH2	160.98	(-3.09)	159.48	(-1.59)	159.99	(-2.10)	158.49	(-0.60)	157.89
CHCCH2CCH	161.47	(-2.80)	160.61	(-1.94)	160.21	(-1.54)	159.35	(-0.68)	158.67
CH3CCCCH	151.90	(-3.27)	150.87	(-2.24)	150.29	(-1.66)	149.26	(-0.63)	148.63
OCCHCH	100.73	(-2.26)	99.60	(-1.13)	100.12	(-1.65)	99.00	(-0.53)	98.47
CH3CH2OOH	-22.52	(0.07)	-22.79	(0.34)	-22.08	(-0.37)	-22.35	(-0.10)	-22.45
CH3CH2CH2CH3	-13.46	(-0.11)	-13.62	(0.05)	-13.23	(-0.34)	-13.37	(-0.20)	-13.57
(CH3)2CHCH3	-14.99	(-0.03)	-15.16	(0.14)	-14.67	(-0.35)	-14.83	(-0.19)	-15.02
CH3OOCCH3	-12.92	(0.02)	-13.22	(0.32)	-12.44	(-0.46)	-12.74	(-0.16)	-12.90
OCOCO	27.06	(-1.76)	25.52	(-0.22)	27.16	(-1.86)	25.66	(-0.36)	25.30
CH3CH2OCH3	-36.21	(-0.27)	-36.39	(-0.09)	-36.08	(-0.40)	-36.27	(-0.21)	-36.48
CH2CCHCCH	157.40	(-2.71)	156.39	(-1.70)	156.38	(-1.69)	155.37	(-0.68)	154.69
c-CHCHCHCHNH	68.98	(-1.88)	68.17	(-1.07)	68.73	(-1.63)	67.92	(-0.82)	67.10
CHCCCCCH	237.50	(-4.81)	235.86	(-3.17)	235.17	(-2.48)	233.53	(-0.84)	232.69
CHCCCCN	216.77	(-3.70)	215.10	(-2.03)	215.27	(-2.20)	213.59	(-0.52)	213.07
Max		(-4.81)		(-3.17)		(-2.48)		(-0.92)	
RMSD		(1.64)		(1.11)		(1.06)		(0.40)	

^a {aug-cc-pVDZ, cc-pVDZ-F12-OptRI, aug-cc-pVDZ/RI}

^b {aug-cc-pVTZ, cc-pVDZ-F12-OptRI, aug-cc-pVTZ/RI}

^c {a'5Z/a'QZ extrapolation}

* efv@vt.edu

Explicitly correlated coupled cluster method for accurate treatment of open-shell molecules with hundreds of atoms

Ashutosh Kumar and Edward F. Valeev*

*Department of Chemistry, Virginia Tech,
Blacksburg, Virginia 24061, United States*

Frank Neese

*Max-Planck-Institut für Kohlenforschung, Kaiser-Wilhelm-Platz 1,
D-45470 Mülheim an der Ruhr, Germany*

(Dated: August 10, 2020)

Abstract

We present a near-linear scaling formulation of the explicitly-correlated coupled-cluster singles and doubles with perturbative triples method (CCSD(T) $_{\overline{\text{F12}}}$) for high-spin states of open-shell species. The approach is based on the conventional open-shell CCSD formalism [M. Saitow et al., J. Chem. Phys. 146, 164105 (2017)] utilizing the domain local pair-natural orbitals (DLPNO) framework. The use of spin-independent set of pair-natural orbitals ensures exact agreement with the closed-shell formalism reported previously, with only marginally impact on the cost (e.g. the open-shell formalism is only 1.5 times slower than the closed-shell counterpart for the C₁₆₀H₃₂₂ n-alkane, with the measured size complexity of ≈ 1.2). Evaluation of coupled-cluster energies near the complete-basis-set (CBS) limit for open-shell systems with more than 550 atoms and 5000 basis functions is feasible on a single multi-core computer in less than 3 days. The aug-cc-pVTZ DLPNO-CCSD(T) $_{\overline{\text{F12}}}$ contribution to the heat of formation for the 50 largest molecules among the 348 core combustion species benchmark set [J. Klippenstein et al., J. Phys. Chem. A 121, 6580 (2017)] had root-mean-square deviation (RMSD) from the extrapolated CBS CCSD(T) reference values of 0.3 kcal/mol. For a more challenging set of 50 reactions involving small closed- and open-shell molecules [G. Knizia et al., J. Chem. Phys. 130, 054104 (2009)] the aug-cc-pVQ(+d)Z DLPNO-CCSD(T) $_{\overline{\text{F12}}}$ yielded a RMSD of ~ 0.4 kcal/mol with respect to the CBS CCSD(T) estimate.

I. INTRODUCTION

One of the central problems limiting the application of accurate *am initio* methods to large molecular systems is their high computational complexity. For example, the operation and storage requirements of the coupled cluster singles and doubles with perturbative triples[1] method (CCSD(T)) — considered to be the “gold standard” of quantum chemistry — scale as $\mathcal{O}(N^7)$ and $\mathcal{O}(N^4)$ respectively, with N proportional to the system size (e.g. number of electrons or atoms). However, this steep scaling is clearly unphysical, especially for insulators, since the dynamical electron correlation is a local phenomenon [2, 3]; correlation energy of two well-separated electrons decays as R^{-6} , where R is the distance between the centroids of the respective 1-electron states. This problem arises due to the unstructured

* efv@vt.edu

(thus, often delocalized) nature of the reference orbitals (e.g., Hartree-Fock (HF)) which results in the appearance of many non-negligible wave function parameters.

The use of *localized* occupied and unoccupied orbitals allows to reveal the sparsity of the wave function and the Hamiltonian operator. Whereas most localization methods for occupied orbitals result in similar performance, the established strategies for constructing localized unoccupied orbitals differ strongly in the performance and technical complexity; here we only focus on the two pertinent examples. The projected atomic orbitals[4–6] (PAOs) introduced by Pulay and Saebø are inexpensive to construct but due to their nonorthogonality and linear dependence require orthogonalization within each orbital and pair “domain”; the PAO technology was developed by Schütz, Werner and co-workers into a large toolkit of linear scaling correlated methods[7–11]. Unfortunately robust application of PAO-based methods requires the use of relatively large domains[12–15] (20-30 atoms / electron pair) which pushes the crossover with conventional methods to very large molecules. Pair-natural orbitals (PNOs) is another representation of the unoccupied space that for each electron pair is far more compact than the comparable PAO pair domain due to the use of the approximate pair correlation amplitudes. Originally introduced by Edmiston and Krauss in 1965[16], the PNOs were developed in 1970s by Meyer,[17, 18] Ahlrichs, Kutzelnigg, and Staemmler[19].

Although regarded as impractical due to the costs of transforming the Hamiltonian to the PNO basis the PNO method was revived by Neese and co-workers by leveraging the local density-fitting and other approximations[12, 20–22] also used to power the PAO-based methods. The initial *Local* PNO (LPNO) CC theory developed by some of us, after successive rounds of improvement has now evolved into the state-of-the-art near-linear-scaling *Domain* based LPNO (DLPNO) CC[13, 23] methods which are characterized by the use of (1) both PAO (intermediate) and PNO representations, (2) Hilbert-space measures for distance between orbitals[13], (3) *SparseMap*[13] representation of (block-)sparse tensors in terms of binary index-to-domain maps for compact specification of structure and algorithms, (4) hierarchy of pair-screening approximations, etc; similar traits apply to the work of Werner *et al.* [14, 24] and Tew, Helmich and Hättig[25, 26]. These formalisms are fundamental and permit evaluation of other properties such as analytic nuclear gradients[27, 28], excitation energies [29–35], electron attachment/detachment energies[36–38] and response properties[15, 39]. It is also possible to apply the PNO formalism in the context of multi-

configuration methods[40–43]. The closed-shell DLPNO-CCSD(T) method can now regularly calculate energies of protein fragments consisting of a few thousand atoms on a single multi-core computer in a matter of few days[23]. However, most of the interesting and useful chemical phenomena almost always involve open-shell molecular systems like organic radicals, transition metal compounds etc. For the sake of brevity it is not possible to recap the rich history of developments of the single-reference coupled-cluster methods applicable to open-shell systems, without and with spin adaptation;[44–49] interested readers are referred to a number of excellent reviews[50–53] However, extension of the DLPNO-CC methods to the treatment of high-spin open-shell systems has been relatively recent. Hansen, Neese and co-workers extended the LPNO-CC methodology to the open-shell regime in 2011 using quasi-restricted orbitals (QROs)[54] as reference orbitals, with multiple sets of PNOs (for different spin components)[55], resulting in a number of technical problems like multiple integral transformations and PNO overlap matrices, unbalanced treatment of closed- and open-shell species etc. Saitow and co-workers were able to resolve a majority of these issues through the recently developed open-shell DLPNO-CCSD method[56] by using a restricted open-shell HF (ROHF) framework, where the PNOs are generated through the diagonalization of pair-specific 1-electron reduced-density matrix (RDM) obtained from the second-order N-electron valence perturbation theory (NEVPT2). The advantages associated with this approach would be discussed specifically, later in the manuscript. Guo and co-workers recently extended the open-shell DLPNO-CCSD method to perturbative triples in a linear scaling fashion[57]. In similar works, Werner implemented a parallel and efficient near-linear scaling open-shell spin-restricted MP2[58] and more recently, both (spin-) restricted and unrestricted variants of CCSD model[59] where the PNOs were obtained through 1-RDMs of second-order Møller-Plesset perturbation theory (MP2).

However, reduction of the computational complexity is not solely sufficient for practical application of reduced-scaling CC methods. The slow convergence of molecular properties with respect to the basis set quality must also be addressed. For example, the basis set error of atomic correlation energy decreases as $\mathcal{O}[(L_{\max} + 1)^{-3}]$, for a basis set saturated to angular momentum L_{\max} due to the use of Slater determinants as the basis.[60] Explicitly correlated R12/F12 methods,[61–71] in which explicit dependence on the interelectronic distances (r_{ij}) are included in the wave function, are a robust way to reduce the basis set error with only a modest increase in the computational expenses, for example the MP2-R12 methods

pioneered by Kutzelnigg[61] reduced the basis set errors in atoms to $\mathcal{O}[(L_{\max} + 1)^{-7}]$ [72]. This makes these methods an attractive alternative to the extrapolation based methods, which often require very large basis set calculations[73].

Unsurprisingly, recent years have seen numerous developments in the reduced-scaling explicitly correlated coupled-cluster methods. Werner and Krause did a comparative analysis on different choices of representations of the unoccupied space (PAOs, PNOs, orbital specific virtuals (OSVs)[74]) in the explicitly correlated CCSD theory[75]. Tew and Hättig implemented the reduced-scaling variants of explicitly correlated MP2 and CCSD methods utilizing PNOs[25, 26, 76, 77]. Werner and co-workers recently came up with an efficient parallel implementation of explicitly correlated PNO based MP2 and CCSD methods[24, 78]. Some of us recently implemented the near-linear-scaling DLPNO-MP2-F12[79] and DLPNO-CCSD(T) $_{\overline{\text{F12}}}$ methods[80] utilizing the *SparseMap* infrastructure.

Unfortunately, the PNO-based explicitly correlated coupled-cluster methods to open-shell species are not yet readily available. Werner and co-workers recently used a simulation code to test the efficiency of the PNOs obtained from his PNO-RMP2 model in correlated PNO-RCCSD-F12 calculations[58]. Here we report the first *production-quality* implementation of the DLPNO-CCSD(T) $_{\overline{\text{F12}}}$ method for open-shell high-spin molecular species. It leverages the existing open-shell DLPNO-CCSD(T) method and the closed-shell DLPNO-F12 infrastructure while maintaining the near-linear scaling behavior observed for the closed-shell calculations. This manuscript is structured as follows: Section II introduces the formalism of explicitly correlated DLPNO-CCSD(T). Computational details are provided in Sec. III. In Sec. IV, we assess the performance of the new method with respect to robustness, scaling with the system size, and precision. We summarize our findings in Sec. V.

II. FORMALISM

This work utilizes the DLPNO framework to formulate a near-linear scaling perturbative coupled-cluster F12 model, CCSD(T) $_{\overline{\text{F12}}}$ [71, 81]. Some of us implemented the closed-shell DLPNO-CCSD(T) $_{\overline{\text{F12}}}$ method in the ORCA quantum chemistry package[82] in 2018[80] and here we extend it to the case of high-spin open-shell states. This work can also be seen as a reduced-scaling extension of the open-shell canonical CCSD(T) $_{\overline{\text{F12}}}$ method, implemented by Zhang and Valeev[71]. In this section, we take a brief look at the formalism of CCSD(T) $_{\overline{\text{F12}}}$

along with the DLPNO approximations.

A. The PNO-based CCSD(T) $_{\overline{\text{F12}}}$ Method

The CCSD(T) $_{\overline{\text{F12}}}$ energy consists of four contributions:

$$E_{\text{CCSD(T)}_{\overline{\text{F12}}}} = E_{\text{CCSD}} + E_{(\text{T})} + E_{(2)_\text{S}} + E_{(2)_{\overline{\text{F12}}}}, \quad (1)$$

where the first two terms sum up to the conventional CCSD(T) energy, and the third and fourth terms correct for the basis set incompleteness of the reference and CCSD correlation energies, respectively. The CCSD(T) correlation energy for open-shell species has already been implemented recently by Guo et al.[57] in a near-linear scaling fashion; since the $E_{(2)_\text{S}}$ does not require reduced-scaling approximations, we thus focus solely on the reduced-scaling formulation of the last term, $E_{(2)_{\overline{\text{F12}}}}$.

The $E_{(2)_{\overline{\text{F12}}}}$ energy is obtained via the second-order Hylleraas functional[83]:

$$E_{(2)_{\overline{\text{F12}}}} = \langle 1_{\text{F12}} | \hat{H}^{(0)} | 1_{\text{F12}} \rangle + \langle \bar{0} | \hat{H}^{(1)} | 1_{\text{F12}} \rangle + \langle 1_{\text{F12}} | \hat{H}^{(1)} | \bar{0} \rangle, \quad (2)$$

where $|\bar{0}\rangle$ and $\langle\bar{0}|$ are the right and left CCSD wave functions respectively and $|0\rangle$ refers to the reference determinant,

$$|\bar{0}\rangle = \exp(\hat{T})|0\rangle \quad (3)$$

$$\langle\bar{0}| = \langle 0|(1 + \hat{\Lambda})\exp(-\hat{T})|. \quad (4)$$

Using the notation of $i, j, k, ..$ for active occupied orbitals and $a, b, c, ..$ for unoccupied orbitals, the \hat{T} operator within the framework of DLPNO-CCSD theory can be written as,

$$\hat{T} \equiv \hat{T}_1 + \hat{T}_2 \equiv t_{a_i}^i \tilde{a}_i^{a_i} + \frac{1}{(2!)^2} t_{a_{ij}b_{ij}}^{ij} \tilde{a}_{ij}^{a_{ij}b_{ij}}. \quad (5)$$

where $\tilde{a}_i^{a_i}$ and $\tilde{a}_{ij}^{a_{ij}b_{ij}}$ are the one and two-particle excitation operators, a_{ij} refer to the (doubles) PNOs associated with the orbital pair ij , and a_i refer to the orbital-specific unoccupied orbitals obtained as the PNOs of the ‘‘diagonal’’ ii pairs (these ‘‘singles PNOs’’ are screened tighter than the standard doubles PNOs). As in the conventional CCSD(T) method itself, the $\hat{\Lambda}$ operator (which makes the CCSD Lagrangian variational w.r.t. wave function parameters[84]) is approximated by \hat{T}^\dagger . [85] However, it should be noted that the Λ -CCSD(T) method where one needs to solve for an additional set of $\hat{\Lambda}$ amplitude equations, gives more

accurate energies than the conventional CCSD(T) method, specially when the molecules are far from their equilibrium geometries[86], albeit at almost twice the computational cost. In the CCSD(T) $_{\overline{\text{F12}}}$ method, a Löwdin partitioning of the similarity transformed CCSD Hamiltonian matrix $\bar{H} \equiv \exp(-\hat{T})\hat{H}\exp(\hat{T})$ is carried out where the zeroth-order Hamiltonian in Eq. (2) is chosen to be the Fock operator (\hat{F}) while $\hat{H}^{(1)}$ is defined as \bar{H} . This choice ensures no coupling between the $E_{(\text{T})}$ and $E_{(2)\overline{\text{F12}}}$ corrections[81] and thus the CCSD(T) energy is not affected by the presence of explicitly-correlated terms. This makes the CCSD(T) $_{\overline{\text{F12}}}$ formalism quite favorable formally and computationally compared to the iterative CC-R12 methods [68, 87–91]. The perturbative F12 models also offer advantages for incorporating orbital optimizations (see the recent work of Kats and Tew[92]). However, for systems where the coupling between the \hat{T} amplitudes and the F12 geminal operator is strong the iterative CC-R12 methods offer a clear advantage, as the perturbative F12 models treat such coupling to finite, rather than infinite, order. The first-order explicitly correlated wave function (Eq. (2)) can be expressed in terms of geminal functions,

$$|1_{\text{F12}}\rangle \equiv \frac{1}{2!} \sum_{ij} |\hat{\gamma}_{ij}^{ij}\rangle, \quad (6)$$

$$|\hat{\gamma}_{ij}^{ij}\rangle = \frac{1}{2!} \bar{R}_{\alpha\beta}^{ij} \tilde{a}_{ij}^{\alpha\beta} |0\rangle, \quad (7)$$

where $\bar{R}_{\alpha\beta}^{ij}$ refers to the antisymmetrized form of the matrix element of the geminal correlation factor $f(r_{12})$:

$$R_{\alpha\beta}^{ij} \equiv \langle\alpha\beta|\hat{Q}_{ij}f(r_{12})|ij\rangle. \quad (8)$$

The indices α, β correspond to the full unoccupied space, thus, the first-order wave function of Eq. (6) only consists of pure double excitations and is orthogonal to the reference wave function. Furthermore, the projection operator \hat{Q}_{ij} makes the overlap of the wave function with the standard CCSD excitations to be zero,

$$\hat{Q}_{ij} = 1 - \sum_{a_{ij}b_{ij}} |a_{ij}b_{ij}\rangle\langle a_{ij}b_{ij}|. \quad (9)$$

An alternative projector based on PNO-like geminal spanning orbitals (GSOs) developed by some of us previously is not used in this work[93]. In order to satisfy the first-order cusp condition for the singlet (S=0) and triplet (S=1) pair functions, spin projectors for both the states are added to the geminal correlation factor along with the corresponding geminal

amplitudes of $\frac{1}{2}$ (singlet) and $\frac{1}{4}$ (triplet):

$$R_{\alpha\beta}^{ij} \equiv \langle \alpha\beta | \hat{Q}_{ij} f(r_{12}) (\frac{1}{2}\hat{P}_0 + \frac{1}{4}\hat{P}_1) | ij \rangle. \quad (10)$$

The projectors \hat{P}_0 and \hat{P}_1 that project into the singlet and triplet states respectively can be written as:

$$\hat{P}_0 = |\alpha\beta\rangle_0 \langle \alpha\beta|_0 \quad (11)$$

$$\hat{P}_1 = |\beta\beta\rangle \langle \beta\beta| + |\alpha\beta\rangle_1 \langle \alpha\beta|_1 + |\alpha\alpha\rangle \langle \alpha\alpha| \quad (12)$$

where

$$|\alpha\beta\rangle_0 = \frac{1}{\sqrt{2}} \{ \alpha(1)\beta(2) - \beta(1)\alpha(2) \}, \quad (13)$$

$$|\alpha\beta\rangle_1 = \frac{1}{\sqrt{2}} \{ \alpha(1)\beta(2) + \beta(1)\alpha(2) \}. \quad (14)$$

we used the Slater geminal correlation factor[64], $f(r_{12}) = (1 - \exp(-\gamma r_{12})/\gamma)$, approximated with a fit to 6 Gaussian geminals[94]. Optimized (empirical) values of γ for different orbital basis sets are available in the literature[94–96].

Finally, the second-order F12 correction energy is obtained from Eq. (2) by substituting the first-order explicitly correlated wave function,

$$E_{(2)\overline{\text{F12}}} = \sum_{i<j} 2\tilde{V}_{ij}^{ij} + \tilde{B}_{ij}^{ij}. \quad (15)$$

The intermediates \tilde{V}_{ij}^{ij} come from the $\langle \bar{0} | \hat{H}^{(1)} | 1_{\text{F12}} \rangle$ and $\langle 1_{\text{F12}} | \hat{H}^{(1)} | \bar{0} \rangle$ terms of the Eq. (2) with $\hat{H}^{(1)} = \bar{H}$, and thus depend on the \hat{T} amplitudes,

$$\tilde{V}_{ij}^{ij} \equiv V_{ij}^{ij} + \frac{1}{2} (V_{a_{ij}b_{ij}}^{ij} + C_{a_{ij}b_{ij}}^{ij}) t_{ij}^{a_{ij}b_{ij}} + V_{ia_j}^{ij} t_j^{a_j} + V_{a_{ij}i}^{ij} t_i^{a_i}, \quad (16)$$

$$V_{p_{ij}q_{ij}}^{ij} \equiv \frac{1}{2} \bar{R}_{\alpha_{ij}\beta_{ij}}^{ij} \bar{g}_{p_{ij}q_{ij}}^{\alpha_{ij}\beta_{ij}}, \quad (17)$$

$$C_{a_{ij}b_{ij}}^{ij} \equiv F_{a_{ij}}^{\alpha_{ij}} \bar{R}_{\alpha_{ij}b_{ij}}^{ij} + F_{b_{ij}}^{\alpha_{ij}} \bar{R}_{a_{ij}\alpha_{ij}}^{ij}, \quad (18)$$

where p_{ij}, q_{ij} refer to the orbitals of the orbital basis set (OBS) (unoccupied + occupied) corresponding to pair ij . The intermediate \tilde{B}_{ij}^{ij} appears as a result of the resolution of $\langle 1_{\text{F12}} | \hat{H}^{(0)} | 1_{\text{F12}} \rangle$ term with $\hat{H}^{(0)} = \hat{F}$,

$$\tilde{B}_{ij}^{ij} \equiv B_{ij}^{ij} - X_{ij}^{ik} F_k^j - X_{ij}^{kj} F_k^i, \quad (19)$$

$$B_{ij}^{ij} \equiv \bar{R}_{\alpha_{ij}\beta_{ij}}^{ij} F_{\gamma_{ij}}^{\beta_{ij}} \bar{R}_{ij}^{\alpha_{ij}\gamma_{ij}}, \quad (20)$$

$$X_{ij}^{ij} \equiv \frac{1}{2} \bar{R}_{\alpha_{ij}\beta_{ij}}^{ij} \bar{R}_{ij}^{\alpha_{ij}\beta_{ij}}. \quad (21)$$

The excitations onto the full unoccupied space (α, β) are taken into account through the addition of a new complementary auxiliary basis set (CABS)[66]. From Eqs. (19) and (21),

$$\tilde{B}_{ij}^{ij} \leftarrow X_{ij}^{ik} F_k^j \equiv \frac{1}{2} \bar{R}_{\alpha_{ik}\beta_{ik}}^{ik} \bar{R}_{ij}^{\alpha_{ij}\beta_{ij}}, \quad (22)$$

construction of the \tilde{B}_{ij}^{ij} intermediate involves coupling of the ij pair with all other pairs ik through the corresponding PNO overlap matrices. However, consistent with our earlier work on the LPNO-CCSD-F12 method[93], the following approximation is invoked (to decouple the pairs),

$$X_{ij}^{ik} F_k^j \approx \frac{1}{2} \bar{R}_{\alpha_{ij}\beta_{ij}}^{ik} \bar{R}_{ij}^{\alpha_{ij}\beta_{ij}} F_k^j \equiv X_{ij}^{ij_F}, \quad (23)$$

where j_F refers to the Fock-transformed occupied orbitals obtained through linear transformation of occupied orbitals with the occupied-occupied block of the Fock matrix. For the evaluation of the intermediate B , two approximations were employed: a) the D approximation which avoids the computation of the CABS-CABS block of the exchange matrix without the addition of any significant errors[79] b) the standard approximation (SA) which drops the CABS terms appearing in the contraction of the V intermediate with T amplitudes which only introduces errors smaller than the residual basis set incompleteness error (BSIE)[70, 71, 97].

Finally, the spin-adaptation of Eq. (15) yields[71]:

$$\begin{aligned} E_{(2)\overline{\text{F12}}} &= \sum_{I<J} \epsilon_{IJ}^{(2)} + \sum_{I,\bar{J}} \epsilon_{I\bar{J}}^{(2)} + \sum_{\bar{I}<\bar{J}} \epsilon_{\bar{I}\bar{J}}^{(2)}, \\ \epsilon_{IJ}^{(2)} &= \frac{1}{2} \tilde{V}_{IJ}^{IJ} + \frac{1}{16} \tilde{B}_{IJ}^{IJ}, \\ \epsilon_{I\bar{J}}^{(2)} &= \frac{3}{4} \tilde{V}_{I\bar{J}}^{I\bar{J}} + \frac{1}{4} \tilde{V}_{\bar{J}I}^{I\bar{J}} + \frac{9}{64} \tilde{B}_{IJ}^{I\bar{J}} + \frac{3}{64} \tilde{B}_{\bar{J}I}^{I\bar{J}} + \frac{3}{64} \tilde{B}_{I\bar{J}}^{\bar{J}I} + \frac{1}{64} \tilde{B}_{\bar{J}I}^{\bar{J}I}, \\ \epsilon_{\bar{I}\bar{J}}^{(2)} &= \frac{1}{2} \tilde{V}_{\bar{I}\bar{J}}^{\bar{I}\bar{J}} + \frac{1}{16} \tilde{B}_{\bar{I}\bar{J}}^{\bar{I}\bar{J}}. \end{aligned}$$

In the above equation, for the sake of generality, spin dependence of spatial orbitals is assumed: I and \bar{I} refer to the α and β spatial orbitals of orbital i respectively. The prefactors in these terms arise from the cusp coefficients ($\frac{1}{2}$ for singlet and $\frac{1}{4}$ for triplet). We have derived the pair-specific expressions of the F12 intermediates from the canonical equations

provided in the supplementary material of our earlier work[71]. Since this work is based on ROHF-like reference determinants, spatial orbitals for both α and β spins are identical. While DOMOs appear in both the spins as occupied orbitals, SOMOs appear as occupied orbitals for the α spin, and as virtual orbitals for the β spin. In this work, we have implemented a UHF (unrestricted HF) style F12 correction for all the pairs. Thus, F12 corrections for a given DOMO-DOMO pair involve calculations over three spin cases ($\alpha-\alpha$, $\alpha-\beta$, $\beta-\beta$) while SOMO-DOMO and SOMO-SOMO pairs required two ($\alpha-\alpha$, $\alpha-\beta$) and one ($\alpha-\alpha$) spin evaluations respectively. Efficient reduced-scaling evaluation of the F12 intermediates within the *SparseMaps* framework is described next[13].

B. The DLPNO Approximations

1. Orbital domains

All occupied molecular orbitals must be localized to minimize their spatial extent. For closed- and open-shell species the canonical Hartree-Fock and quasi restricted orbitals (QROs)[54] were used as the input orbitals for the Foster-Boys[98] localization algorithm. It should be noted that DOMOs and SOMOs must be localized separately.

Projected atomic orbitals (PAOs) were used as an intermediate basis for the unoccupied orbital space. The PAOs, $\{\tilde{\mu}\}$, are obtained by projecting out the contribution of occupied orbitals, $\{i\}$, from the atomic orbitals, $\{\mu\}$,

$$|\tilde{\mu}\rangle = \left(1 - \sum_i |i\rangle\langle i|\right) |\mu\rangle. \tag{24}$$

The PAOs are generally more localized than their canonical counterparts, and only a spatially-compact subset of them is required to accurately describe the correlation amplitudes associated with a given (localized) occupied orbital (or a set of such orbitals). For a given occupied orbital i , only those PAOs are chosen are in its domain whose differential overlap integral (DOI)[13] with i is greater than the T_{CutDO} threshold,

$$\text{DOI}_{i\tilde{\mu}} \equiv \sqrt{\int d\mathbf{x} |\phi_i(\mathbf{x})|^2 |\phi_{\tilde{\mu}}(\mathbf{x})|^2}. \tag{25}$$

The DOI is a measure of “distance” in Hilbert space between the orbital densities, $|\phi_i(\mathbf{x})|^2$ and $|\phi_{\tilde{\mu}}(\mathbf{x})|^2$; it can be efficiently evaluated in a linear scaling fashion using standard quadrature

techniques[13]. The PAO domains are “atom-complete” in the sense that if one or more of an atom’s PAO is included in a given domain, all other PAOs associated with that atom are added as well. Consequently, pair, triples, etc. domains are constructed from the union of the individual domains.

Both localized MOs or PAOs are sparsified further to neglect contributions from AOs with coefficient less than threshold T_{CutC} ; this sparsification is also atom-complete, i.e. if an AO contributes with coefficient greater than T_{CutC} then contributions from all other AOs of that atom are included. Of course, the AOs need to be normalized first in order to take advantage of this sparsity.

For the DLPNO-F12 procedure to be linear scaling the domains for occupied and CABS AOs must also be introduced. These are defined as follows[79]. For a given orbital i the domain of CABS AOs includes all atoms which have one or more PAO with DOI to i of not less than $T_{\text{CutDO}}/10$. (note that we did not use PAO-like representation for the CABS basis). The CABS domain for pairs are obtained by taking a union of the individual CABS AO domains. The domain of occupied orbitals (including core) for a given *active* occupied orbital i includes all orbitals with DOI to that orbital of not less than $T_{\text{CutDO}}/10$. Thus, the domain sizes of occupied, PAO, and CABS AOs are controlled by a single parameter T_{CutDO} ; as it is lowered the domains grow roughly logarithmically.

The AO domains for local density fitting were defined as in previous work[13].

2. *Pair-natural orbitals*

PNOs are much more compact than PAOs and are hence employed as the final representation of the unoccupied space. In this work, PNOs are obtained by the diagonalization of the NEVPT2 pair-densities constructed in the PAO space and (as before) are truncated based on the parameter T_{CutPNO} . [56] The choice of the NEVPT ansatz ensures that (1) a single set of PNOs (NEV-PNOs) is obtained which converges to the MP1-PNOs at the closed-shell limit since all the excitations involving the SOMOs disappear; (2) the wave function is intruder-state free as the zeroth-order wave function (Dyall’s model Hamiltonian[99]), unlike the Fock operator, includes the complete two-body interaction in the SOMO space; (3) the pair energies and the pair wave function are invariant to the unitary transformations within the DOMO, SOMO and (pure) unoccupied spaces.

Thus, the use of NEV-PNOs offers significant advantages over the PNOs generated from UMP1 pair-densities[55] which can suffer from the intruder-state problem. Also, in such an approach, three sets of PNOs are generated, resulting in (at least three times as many) integral transformations from the PAO to PNO space. Furthermore, it is quite difficult to match the closed-shell results with RHF based DLPNO implementations even after using the same T_{CutPNO} values since the densities of the same-spin and opposite-spin pairs would have different truncations. This often results in an unbalanced treatment of closed- and open-shell states, leading to errors in reaction energies, singlet-triplet gaps etc. Finally, even at zero PNO truncation, the correlation energies obtained doesn't match with the canonical values: for diagonal pairs of the same spin, PNOs cannot be generated (zero density), resulting in the removal of terms that depend on them in the CCSD residual equations[56].

3. Pair-screenings

The CCSD(T) $_{\overline{\text{F12}}}$ energy evaluation can be made linear-scaling only if the number of correlated electron clusters (pairs, triples, etc.) grows linearly with the system size. In this regard, a hierarchy of approximations have been employed, beginning with the *pair-prescreening* step, where a pair ij is neglected if $\text{DOI}_{ij} < T_{\text{CutDOI}_{ij}}$ and dipole-approximated semi-local NEVPT2 energy (E_{PreScr}) [42] is smaller than $T_{\text{CutPre}} \cdot E_{\text{PreScr}}$ for that pair is added to the correlation energy. Consistent with the RHF implementation, a two-step guess procedure (*crude* and *fine*) is then followed. The domains in the *crude* guess step are chosen to be smaller than the ones used in the *fine* guess stage by using scaled versions of the *fine* guess truncation parameters, $T_{\text{CutDO}_{\text{Crude}}} = 2 \times T_{\text{CutDO}}$, $T_{\text{CutMKN}_{\text{Crude}}} = 10 \times T_{\text{CutMKN}}$. The pairs are classified on the basis of their correlation energies (ϵ_p) as *Crude_CC* ($\epsilon_p > T_{\text{CutPairs}}$), *Crude_PT2* ($\epsilon_p > T_{\text{CutPairs}_{\text{MP2}}}$) and *weak* pairs (remaining). Both *Crude_CC* and *Crude_PT2* pairs enter the *fine* guess stage, where the above process is repeated (albeit with larger domains) and a CC pair list is obtained with the energies of *weak* and *PT2* pairs added to the total correlation energy. This two-step guess construction minimizes the computation of three-index integrals while maintaining the accuracy of the correlation energies. It should also be noted that pairs involving SOMOs do not take part in the *pre-screening* and *crude* guess steps due to large truncation errors[56]. Finally, PNOs are generated and then truncated for the CC pairs followed by the addition of a PNO truncation correction obtained from

the difference between semi-local NEVPT2 correlation energies in the PAO and (truncated) NEV-PNO representations. Finally, all the integrals are transformed to the truncated PNO basis and CC residual equations are solved.

Since the explicit correlation treatment is expected to be important for only spatially-close pairs, just like in the closed-shell formalism[79] only a subset of the CC pairs (ij), defined by the criterion, $\text{DOI}_{ij} > 30 \times T_{\text{CutDOIj}}$ are treated as the F12 pairs. Furthermore, *fine* guess maps were used for defining the domain sizes used in the F12 specific integral transformations.

4. SOMO handling

Since SOMOs appear as both occupied (α spin) and unoccupied orbitals (β spin), they need to be included in the occupied, PAO, and PNO domains for the integral transformations. In this work, all N_{SOMO} SOMOs are included in every PAO domain of the occupied orbitals and the PAO-PNO transformation matrix for every pair is augmented by an N_{SOMO} by N_{SOMO} identity matrix. This avoids the *integral-direct* transformations of a number of integral classes which differ only by zero or more SOMOs: for example, the $(I\bar{A}_{IJ}|J\bar{B}_{IJ})$ integral batch, in which SOMOs appear in every orbitals space, also contains other required integral batches, such as $(IA_{IJ}|JB_{IJ})$, $(I\bar{A}_{\bar{I}\bar{J}}|\bar{J}\bar{B}_{\bar{I}\bar{J}})$, $(I\bar{A}_{\bar{I}\bar{J}}|\bar{J}B_{\bar{I}\bar{J}})$, etc. This strategy enables the re-use of optimized integral transformation routines of the closed-shell DLPNO infrastructure. Replicating SOMOs in different integral classes and PNOs of every pair does introduce some redundancy which can become a problem if the number of SOMOs is large. Also, each SOMO shares the same orbital domain formed by taking an union of the domains of individual SOMOs since the NEVPT2 energy expression of pairs (in the PAO basis) with SOMOs include terms with summations over all SOMO-SOMO pairs [56].

As discussed before, the DLPNO-F12 procedure requires the construction of occupied-occupied domains. We make sure that all the SOMOs are included in each of these domains. This ensures that the local OBS space for a pair i.e. local occupied orbitals + PNOs, become independent of the spin, making the local CABS space which is orthogonal to the local OBS space spin-independent as well.

5. F12 integral transformations

Integral transformations are one of the most compute-intensive parts of a perturbative F12 correction model like DLPNO-CCSD(T) $_{\overline{\text{F12}}}$. Since our F12 calculations utilize two spaces (OBS, CABS) and 5 integral kernels: $\frac{1}{r_{12}}, f_{12}, f_{12}^2, \frac{f_{12}}{r_{12}}, [f_{12}, [\hat{T}, f_{12}]]$, ten sets of 3-index 2-electron integrals ($ip_{ij}|K|V_{ij}$) need to be evaluated, with K one of the 5 integral kernels and p either the OBS or CABS space index. In addition, ($p_{ij}a_{ij}|\frac{1}{r_{12}}|V_{ij}$) integrals (where a_{ij} is the PAO index), Fock-transformed (kernel: f_{12} ; space: OBS, CABS; spin: α, β) and t_1 transformed[80] (kernel: $\frac{1}{r_{12}}, \frac{f_{12}}{r_{12}}$; space: OBS; spin: α, β) integrals are also required, resulting in a total of **19** 3-index integral transformations.

Evaluation of these 3-index integrals is mostly identical to the closed-shell DLPNO F12 formalism[79, 80] using the pair-extended SparseMaps.[13] Namely, the domain of an occupied orbital i is augmented with the domains of all those occupied orbitals j , if the pair ij exists in the F12 pair list. Consequently, for a given pair ij , integrals of i and j are sieved out from these pair-extended integrals and recombined through local density fitting, followed by their transformation to the PNO basis to evaluate ij -specific intermediates.

However, evaluation of the ($p_{ij}a_{ij}|\frac{1}{r_{12}}|V_{ij}$) integrals was significantly improved compared to the closed-shell DLPNO-F12 formalism as follows. As is the case for all 3-index integrals in the DLPNO framework,[13] integral-direct transformation is driven by the density-fitted atomic orbitals X : for each batch of X a set of integrals ($\mu_X\nu_X|X$) is computed and then transformed to the PAO basis. For the ($p_{ij}a_{ij}|\frac{1}{r_{12}}|V_{ij}$) integral evaluation in the closed-shell DLPNO CC-F12 formalism[80] the sets of AOs μ_X were calculated by the following composition of sparse maps:[13] $\mathbf{L}(X \rightarrow p) \subset \mathbf{L}(p \rightarrow \mu)$ where $\mathbf{L}(X \rightarrow p) \equiv \mathbf{L}(X \rightarrow i) \subset \mathbf{L}(i \rightarrow j) \subset \mathbf{L}(j \rightarrow p)$, whereas ν_X was constructed as: $\mathbf{L}(X \rightarrow p) \subset \mathbf{L}(p \rightarrow a) \subset \mathbf{L}(a \rightarrow \nu)$ where $\mathbf{L}(p \rightarrow a) \equiv \mathbf{L}(p \rightarrow i) \subset \mathbf{L}(i \rightarrow j) \subset \mathbf{L}(j \rightarrow a)$. Here, \subset refers to the ‘‘chaining’’ operation, for example, chaining of two maps $\mathbf{L}_1(f \rightarrow g)$ and $\mathbf{L}_2(g \rightarrow h)$ produces another map $\mathbf{L}_3(f \rightarrow h)$, where a given h is included in map L_3 only when there is a g in map L_1 that is connected to h in L_2 map. In the data structure sense, a sparse map L can be thought of as a **vector of vectors** which allows the individual elements of this structure to have different sizes based on the ‘‘connectedness’’ of that given orbital which is of course determined by metrics like DOI. Such definition of the ν_X domain including the ‘‘chain’’ of $\mathbf{L}(X \rightarrow p)$ and $\mathbf{L}(p \rightarrow a)$ (pair-extended) maps turns out to be too conservative, leading to

excessive storage and operational costs. This problem was avoided in this work by evaluating the $\mathbf{L}(X \rightarrow a)$ maps in the same fashion as the auxiliary to OBS maps: $\mathbf{L}(X \rightarrow a) \equiv \mathbf{L}(X \rightarrow i) \subset \mathbf{L}(i \rightarrow j) \subset \mathbf{L}(j \rightarrow a)$. Even though both approaches have linear cost in system size, the new algorithm has a significantly reduced prefactor without sacrificing the accuracy.

III. COMPUTATIONAL DETAILS

All numerical experiments were performed using a developmental version of ORCA 4.2. ROHF and quasi restricted orbitals (QROs) were used as the reference orbitals in UHF based computations. Core orbitals were kept doubly occupied in all correlated computations. Evaluation of the B F12 intermediate followed the F12/D approximation.[79] A number of orbital basis sets (OBS) were utilized in this work: aug-cc-pV[X]Z and aug-cc-pV[X](+d)Z basis sets of Dunning et al.[100], F12-optimized basis sets of Peterson et al.[96], cc-pV[X]Z-F12, with $X = D, T$, where X is the cardinal number of the basis set and the def2-family of basis sets developed by Weigend and Ahlrichs[101], def2-TZVP, def2-TZVPP and def2-SVP. For a given OBS, the corresponding density-fitted basis set (DFBS) was used unless stated otherwise[102–104], ex. for aug-cc-pVDZ basis set, aug-cc-pVDZ/RI was used as the auxiliary basis. For the cc-pV[X]Z-F12 basis sets, aug-cc-pV[X]Z/RI was used as the DFBS. In the construction of the CABS space, *uncontracted* def2-TZVPP and def2-QZVPP basis sets were used when the standard optimized cc-pV[X]Z-F12-OptRI[105] basis set ($X=D, T$) family was not available for the given molecular species.

The convergence of the correlation energy with respect to the DLPNO truncation parameters (T_{CutPNO} , T_{CutDO} , T_{CutPairs} , T_{CutMKN}) was assessed for the doublet trityl radical at the B3LYP/def2-TZVPP equilibrium geometry; these computations utilized the {aug-cc-pVDZ, cc-pVDZ-F12-OptRI, aug-cc-pV5Z-RI} {OBS, CABS, DFBS} triplet. The Hartree-Fock orbitals were computed using the `VeryTightSCF` SCF convergence settings of ORCA. The computational scaling with size was assessed for n-alkanes ranging from $\text{C}_{20}\text{H}_{42}$ to $\text{C}_{160}\text{H}_{322}$ at idealized quasilinear geometry using {def2-TZVP, cc-pVDZ-F12-OptRI, def2-TZVP/C} basis set triplet. In these studies the Coulomb operator was approximated by the standard $\mathcal{O}(N^3)$ density-fitting procedure using the def2/J basis set[103], which we will refer to as the coulomb density-fitted basis (CDFBS), while the exchange operator was described by the linear scaling chain of spheres approximation (COSX)[106] used with default grid

parameters.

The accuracy of the present method was analyzed and compared with extrapolation based techniques in heats of formation calculations on a representative set of molecules out of the ANL database of 348 core combustion species[107] and reaction energies of 50 open-shell reactions[108]. Finally, computational timings were reported for some chemically relevant medium and large sized molecules.

All the calculations reported in this work were carried out on multicore nodes (although we utilized only 4 cores) with dual E5-2683v4 2.1GHz (Broadwell) and dual E5-2680v3 2.5GHz (Haswell) processors, each node with a total memory of 512 GB.

IV. RESULTS

A. Convergence of the $\text{CCSD}_{\overline{\text{F12}}}$ correlation energy with respect to the DLPNO truncation parameters

To be usable in chemical applications reduced-scaling methods must allow robust control of precision, hence the errors due to the sparsifying approximations should decay monotonically and rapidly as the truncation parameters approach zero; when all truncation parameters vanish the reduced-scaling method should become equivalent to the canonical counterpart. To this end we performed a systematic analysis of the convergence behavior of the UHF-based DLPNO $\text{CCSD}_{\overline{\text{F12}}}$ correlation energies for the trityl radical in the doublet state, a medium-sized system used previously by some of us to assess the open-shell DLPNO-CCSD method.[56] (the lack of support for density fitting in the open-shell *canonical* CCSD code in ORCA prevented us from using a larger molecule). To be able to compare the canonical and DLPNO results we used the aug-cc-pV5Z-RI as DFBS to minimize the errors introduced due to the density-fitting approximation used in the DLPNO procedure.

Fig. 1a illustrates the convergence behavior of the DLPNO-CCSD (blue) and DLPNO- $\text{CCSD}_{\overline{\text{F12}}}$ (red) valence correlation energies of doublet trityl radical as a function of the PNO truncation parameter, T_{CutPNO} when all other truncation parameters are set to 0. It can be seen that both curves converge monotonically towards their respective canonical correlation energies and at the PNO truncation of 10^{-7} , around 99.86% of the canonical energy is recovered for both the methods. However, the F12 energies show a slower convergence than its

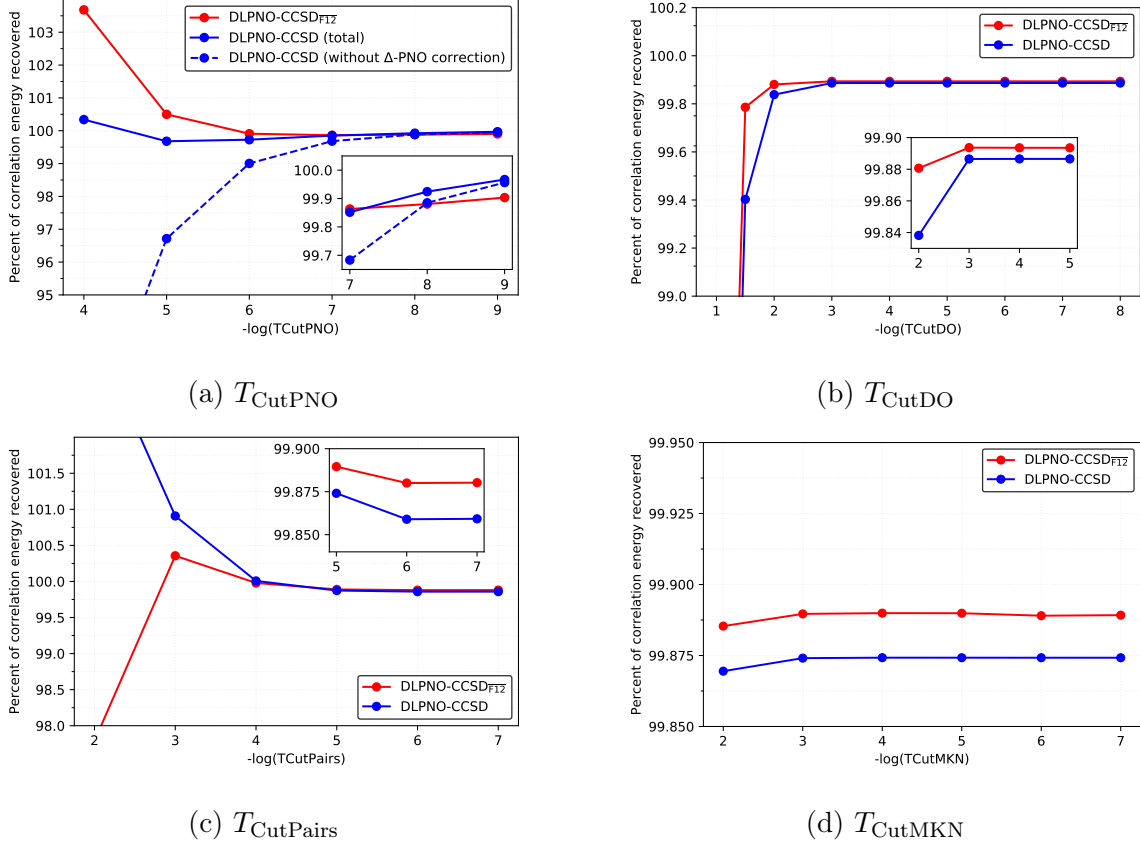


FIG. 1: DLPNO-CCSD and DLPNO-CCSD_{F12} valence correlation energies of doublet trityl radical shown in terms of the percentage of the respective canonical energies, as a function of the truncation parameters. All other truncation parameters are set to zero for (a) and to **TightPNO** settings: $\{T_{\text{CutPNO}} = 10^{-7}, T_{\text{CutDO}} = 5 * 10^{-3}, T_{\text{CutMKN}} = 10^{-4}, T_{\text{CutPairs}} = 10^{-5}\}$ for (b), (c) and (d).

conventional counterpart: at a truncation of 10^{-9} , DLPNO-CCSD recovers around 99.97% while DLPNO-CCSD_{F12} yields a little more than 99.9% of their canonical correlation energies. Also, at looser thresholds, the errors in the F12 energies are higher, which is consistent with the behavior that we observed in the LPNO-CCSD(2)_{F12} method[93]. Note that the errors would be significantly larger in both conventional and F12 CCSD energies if the PNO incompleteness correction ($\Delta - \text{PNO}$)[21] were not included, as illustrated for the CCSD case with the dashed line. Further reduction of the truncation error when $T_{\text{CutPNO}} \leq 10^{-8}$ is possible by reoptimizing the PNOs for the case of the coupled-cluster wave function.[109]

Figure 1b demonstrates the dependence of the DLPNO-CCSD and DLPNO-CCSD_{F12} energies on T_{CutDO} , the truncation parameter that defines the size of PAO domains. All other truncation parameters are set to **TightPNO** settings: $\{T_{\text{CutPNO}} = 10^{-7}, T_{\text{CutDO}} = 5 \times 10^{-3},$

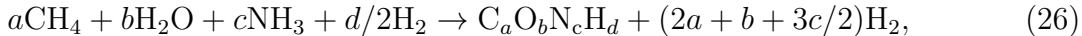
$T_{\text{CutMKN}} = 10^{-4}$, $T_{\text{CutPairs}} = 10^{-5}$ }. Unlike the PNO graph above, both the methods exhibit similar behavior and converge towards the canonical energy from below, with slightly lower errors in the F12 energies, in agreement with the findings of Werner[110] and our observations in the DLPNO-CCSD $_{\overline{\text{F12}}}$ method[80] for closed-shell systems. At $T_{\text{CutDO}} = 10^{-2}$, the % recovery for DLPNO-CCSD and DLPNO-CCSD $_{\overline{\text{F12}}}$ energies are 99.84 and 99.88 respectively while at $T_{\text{CutDO}} = 10^{-3}$, both curves have essentially converged to $\approx 99.89\%$.

Similar convergence behavior is observed for T_{CutPairs} (Fig.1c) and T_{CutMKN} (Fig.1d) truncation parameters with F12 energies recovering a slightly higher percentage of correlation energy near convergence. In Fig.1d, the errors for both the methods are quite small even at $T_{\text{CutMKN}} = 10^{-2}$, which is reflective of the large density-fitting basis set (aug-cc-pV5Z/RI) used in these calculations. On average $\approx 99.86\%$ of the canonical correlation energy is recovered at the **TightPNO** setting.

B. Accuracy studies

1. Heats of formation

The total correlation energy of the doublet triphenyl radical is around 3 Hartrees and even with an overall accuracy of 99.86%, the total error comes to be around 2.7 kcal/mol, much higher than the desired chemical accuracy of 1 kcal/mol. However, most of the chemical phenomena actually depend on relative energies of some kind and not absolute energies. Thus, its important to study the effect of all the DLPNO truncations on the accuracy of relative energy calculations. To this end, we assessed the accuracy of the DLPNO-CCSD(T) $_{\overline{\text{F12}}}$ method for calculating heats of formation of 50 largest compounds out of the ANL database of 344 core combustion species[107]. Following the works of Klippenstein and co-workers[107], we use H₂, CH₄, H₂O and NH₃ as the reference species for the H, C, O, and N elements respectively. Thus, for the formation of C_aO_bN_cH_d species, the following “working reaction” is considered,



and the enthalpy of formation of $C_aO_bN_cH_d$ can be calculated as[111]

$$\begin{aligned}
& \Delta_f H_0^\circ (C_aO_bN_cH_d) \\
&= [a\Delta_f H_0^\circ (\text{CH}_4) + b\Delta_f H_0^\circ (\text{H}_2\text{O}) + c\Delta_f H_0^\circ (\text{NH}_3) \\
& \quad + (d/2 - 2a - b - 3c/2)\Delta_f H_0^\circ (\text{H}_2)] \\
& \quad + [E (C_aO_bN_cH_d) - aE (\text{CH}_4) - bE (\text{H}_2\text{O}) \\
& \quad \quad - cE (\text{NH}_3) + (2a + b + 3c/2 - d/2)E (\text{H}_2)].
\end{aligned} \tag{27}$$

In this work, we are only interested in the contribution of the non-relativistic electronic energy to the heats of formation and E in the above equation will refer to the same. We compare the heats of formation obtained using DLPNO-CCSD(T) $_{\overline{\text{F12}}}$ and CBS extrapolation of canonical CCSD(T) energies within the ANL0 scheme. The extrapolations employed aug'-cc-pVQZ (a'QZ) and aug'-cc-pV5Z (a'5Z) basis sets while using the following formula: $E_{CBS} = E_{a'nZ} + \alpha(E_{a'nZ} - E_{a'(n-1)Z})$. In the primed basis sets (a'QZ), diffuse functions are omitted except the s functions on the H atoms and the s and p functions on the C, N and O atoms. $\alpha = 0.75$ was chosen such that the RMSD between (experimental) ATcT[112] values and the ANL0 predictions were minimized[107]. Also, the extrapolated results using optimized values of α were shown to be in close agreement with the $1/l_{\text{max}}^{3.7}$ extrapolation scheme. The geometries of these 50 molecules were optimized with canonical CCSD(T) using the cc-pVTZ basis set. The energies of 21 closed-shell species (out of 50) were calculated by the RHF-DLPNO-CCSD(T) method. We have used four sets of basis set triplets, {OBS, CABS, DFBS}: {cc-pVDZ-F12, cc-pVDZ-F12-OptRI, aug-cc-pVDZ/RI}, {cc-pVTZ-F12, cc-pVTZ-F12-OptRI, aug-cc-pVTZ/RI}, {aug-cc-pVDZ, cc-pVDZ-F12-OptRI, aug-cc-pVDZ/RI} and {aug-cc-pVTZ, cc-pVDZ-F12-OptRI, aug-cc-pVTZ/RI} with the DLPNO-CCSD(T) $_{\overline{\text{F12}}}$ method using both iterative, (T1),[57, 113] and semi-canonical non-iterative, (T0),[23] variants of the triples correction. From now on, we will refer to the cc-pV[X]Z-F12 and aug-cc-pV[X]Z basis sets as [X]Z-F12 and a[X]Z basis sets, respectively.

The computed DLPNO-CCSD(T) $_{\overline{\text{F12}}}$ and the extrapolated CBS CCSD(T) heats of formation are tabulated in the supplementary information. Consider first the DZ-F12 results (Fig. 2a) with the T0 approximation: the max and RMSD are -2.13 and 0.63 kcal/mol,

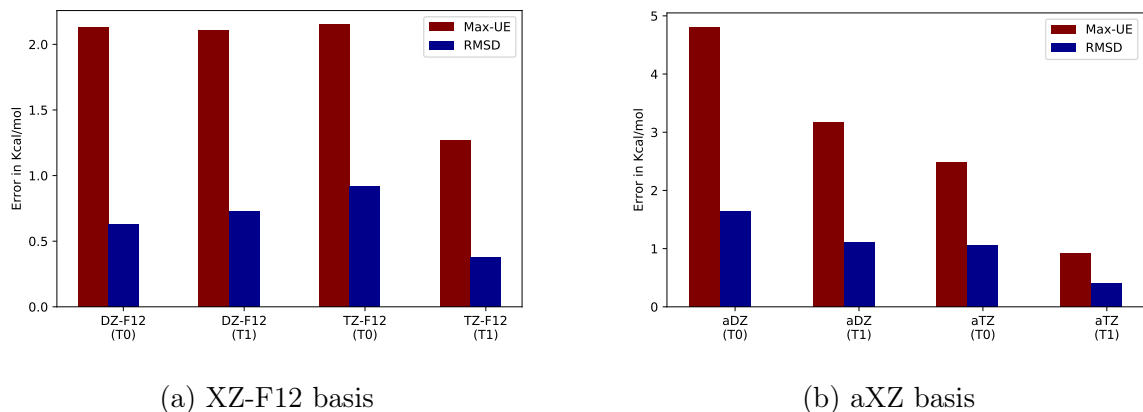


FIG. 2: Max unsigned error and RMSD of the UHF-DLPNO-CCSD(T) $_{\overline{\text{F12}}}$ method with a) cc-pV[D,T]Z-F12 and b) aug-cc-pV[D,T] basis sets. Errors are calculated with respect to the canonical CBS values using the a'5Z/a'QZ extrapolation technique of Ref.[107].

respectively. Quite surprisingly, the more accurate T1 approximation gives higher RMSD for the same basis set: max and RMSD are 2.11 and 0.73 kcal/mol, respectively. With the larger TZ-F12 basis set the corresponding errors (max error, RMSD) for the T0 and T1 approximations are (-2.15, 0.92) and (-1.27, 0.38) kcal/mol, respectively. The errors in the smallest basis set used, aDZ (Fig. 2b) are the largest: (-4.81, 1.64) and (-3.17, 1.11) kcal/mol. On the other hand, the aTZ basis set yields errors of (-2.48, 1.06) and (-0.92, 0.40) kcal/mol for the T0 and T1 approximations, respectively. These results clearly indicate that the less expensive T0 approximation is unable to provide errors within the chemical accuracy and the more accurate T1 approximation should be preferred for these calculations which is consistent with the findings of Liakos et al.[114] Furthermore, the DZ-F12 basis set results with the T0 approximation is at best fortuitous since they are lower than the corresponding TZ-F12 and aTZ errors: (1.73, 0.45) vs (1.77, 0.69) and (2.11, 0.86) kcal/mol, respectively. The DLPNO-CCSD(T1)-F12 method with both TZ-F12 and aTZ basis sets yield RMSD of less than 0.40 kcal/mol at a fraction of the cost of the extrapolated canonical CCSD(T) procedure. However, given the smaller size of the aTZ basis compared to that of TZ-F12 the use of the former seems to be more economical in this case and is cautiously recommended for future applications; a more extensive benchmarking is however warranted.

Fig. 3 compares the errors obtained from canonical CCSD(T) method using a'TZ, a'QZ and a'5Z basis sets with the DLPNO-CCSD(T) $_{\overline{\text{F12}}}$ method using the aTZ basis set. It can be seen that the DLPNO errors are only slightly worse than the canonical a'5Z basis errors:

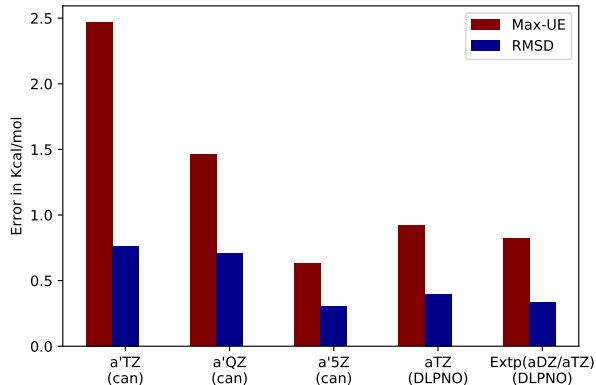


FIG. 3: Max unsigned error and RMSD of canonical CCSD(T) method with a'TZ, a'QZ and a'5Z basis sets and UHF-DLPNO-CCSD(T) $_{\overline{\text{F12}}}$ method with aTZ basis. Extrap refers to the extrapolated results with $1/l_{\text{max}}^3$ scheme. Errors are calculated with respect to the canonical CBS values using the a'5Z/a'QZ extrapolation technique of Ref.[107].

(0.63, 0.30) vs (0.92, 0.40) kcal/mol. Furthermore, we also carried out the simple X^{-3} based extrapolation scheme with the DLPNO-aDZ and DLPNO-aTZ F12 energies and the errors are further reduced to (0.82, 0.33) kcal/mol.

2. Reaction energies

We chose the reaction energies (REs) of 50 “open-shell” reactions originally devised by Knizia et al.[108] as a more challenging benchmark for the DLPNO-CCSD(T) $_{\overline{\text{F12}}}$ method. Out of the 47 molecules involved in these reactions, 17 are open-shell species, which include atoms, 2nd and 3rd period elements in doublet and triplet spin states. Large reaction energies coupled with a strong basis set dependence makes this test set quite challenging for the F12 methods. The aug-cc-pVT(+d)Z (denoted for simplicity as aVTZ) and aug-cc-pVQ(+d)Z (denoted as aVQZ) basis sets were employed as the OBS with cc-pVQZ-F12-OptRI and aug-cc-pVQZ/RI as the CABS and DFBS respectively. Furthermore, due to the higher accuracy requirements and relatively small system size, the more accurate T1 variant of (T) was used with **TightPNO** and **VeryTightPNO** ($\{T_{\text{CutPNO}} = 10^{-8}, T_{\text{CutDO}} = 5 * 10^{-3}, T_{\text{CutMKN}} = 10^{-4}, T_{\text{CutPairs}} = 10^{-5}\}$) truncation settings. ROHF orbitals were used in all of these calculations.

Table I shows the percent recovery of DLPNO-CCSD(T) $_{\overline{\text{F12}}}$ correlation energies of all the molecular species present in the test set (excluding the hydrogen atom) with respect

TABLE I: Total DLPNO-CCSD(T) $_{\overline{\text{PT2}}}$ correlation energies recovered (%) with respect to the canonical values with aVTZ and aVQZ basis sets at TightPNO and VeryTightPNO truncation settings. The numbers in the paranthesis denote the errors in kcal/mol.

	aVTZ				aVQZ			
	TightPNO		VeryTightPNO		TightPNO		VeryTightPNO	
HC1	99.86	(-0.23)	99.97	(-0.04)	99.77	(-0.37)	99.93	(-0.12)
Cl	100.11	(0.15)	100.24	(0.33)	99.85	(-0.20)	99.99	(-0.01)
H2	99.98	(-0.01)	99.98	(-0.01)	99.90	(-0.03)	99.90	(-0.03)
F2	99.87	(-0.49)	99.97	(-0.13)	99.82	(-0.70)	99.91	(-0.36)
H2O	99.96	(-0.08)	99.97	(-0.05)	99.90	(-0.20)	99.92	(-0.15)
HF	99.96	(-0.07)	99.98	(-0.03)	99.88	(-0.23)	99.93	(-0.13)
O	100.39	(0.46)	100.40	(0.47)	100.05	(0.06)	100.05	(0.06)
CH4	99.97	(-0.04)	99.98	(-0.03)	99.91	(-0.14)	99.91	(-0.13)
OH	100.18	(0.27)	100.16	(0.24)	100.00	(0.01)	100.01	(0.01)
CH3	99.98	(-0.02)	99.99	(-0.02)	99.95	(-0.06)	99.96	(-0.06)
CO	99.93	(-0.17)	99.99	(-0.03)	99.86	(-0.35)	99.94	(-0.16)
CO2	99.89	(-0.46)	99.97	(-0.12)	99.83	(-0.73)	99.92	(-0.36)
Cl2	99.76	(-0.71)	99.95	(-0.15)	99.73	(-0.84)	99.91	(-0.29)
CH3Cl	99.87	(-0.38)	99.96	(-0.11)	99.83	(-0.50)	99.91	(-0.25)
S	99.73	(-0.28)	100.04	(0.04)	99.71	(-0.31)	99.95	(-0.05)
H2S	99.80	(-0.30)	99.98	(-0.03)	99.75	(-0.39)	99.92	(-0.12)
NO2	99.91	(-0.45)	99.98	(-0.10)	99.86	(-0.69)	99.92	(-0.39)
O2	100.13	(0.43)	100.07	(0.24)	100.08	(0.27)	100.02	(0.06)
NO	100.02	(0.07)	100.03	(0.10)	99.93	(-0.21)	99.98	(-0.07)
N	100.17	(0.13)	100.17	(0.13)	100.13	(0.10)	100.00	(0.00)
H2O2	99.90	(-0.37)	99.97	(-0.11)	99.84	(-0.57)	99.91	(-0.32)
N2	99.92	(-0.21)	99.99	(-0.03)	99.85	(-0.39)	99.93	(-0.18)
SO3	99.81	(-1.22)	99.95	(-0.35)	99.81	(-1.21)	99.91	(-0.59)
SO2	99.81	(-0.89)	99.95	(-0.23)	99.80	(-0.99)	99.91	(-0.45)
HOCl	99.83	(-0.57)	99.96	(-0.12)	99.81	(-0.64)	99.91	(-0.30)
HNO3	99.82	(-1.17)	99.94	(-0.38)	99.80	(-1.37)	99.88	(-0.78)
N2H4	99.91	(-0.27)	99.96	(-0.11)	99.87	(-0.41)	99.91	(-0.28)
NH2	100.00	(0.00)	99.99	(-0.02)	99.97	(-0.05)	99.96	(-0.05)
Si2H6	99.82	(-0.38)	99.97	(-0.07)	99.80	(-0.43)	99.91	(-0.20)
SiH3	99.81	(-0.19)	99.93	(-0.07)	99.73	(-0.27)	99.85	(-0.15)
SH	99.81	(-0.25)	100.07	(0.08)	99.70	(-0.39)	99.94	(-0.08)
CH3SH	99.85	(-0.42)	99.96	(-0.11)	99.81	(-0.53)	99.91	(-0.25)
CS	99.84	(-0.36)	99.98	(-0.04)	99.77	(-0.55)	99.93	(-0.17)
CH3OH	99.93	(-0.23)	99.97	(-0.10)	99.89	(-0.35)	99.92	(-0.27)
HCHO	99.92	(-0.24)	99.98	(-0.07)	99.86	(-0.40)	99.92	(-0.23)
NH	100.11	(0.12)	100.10	(0.11)	99.94	(-0.07)	99.93	(-0.08)
SiH4	99.85	(-0.17)	99.97	(-0.03)	99.83	(-0.21)	99.91	(-0.10)
Si	99.71	(-0.15)	99.68	(-0.17)	99.92	(-0.04)	99.98	(-0.01)
C2H4	99.94	(-0.15)	99.97	(-0.07)	99.89	(-0.29)	99.92	(-0.21)
CH3CH	99.90	(-0.39)	99.96	(-0.15)	99.86	(-0.58)	99.91	(-0.38)
CS2	99.77	(-0.85)	99.96	(-0.14)	99.72	(-1.03)	99.90	(-0.36)
NH3	99.96	(-0.08)	99.97	(-0.05)	99.90	(-0.17)	99.93	(-0.13)
C	100.23	(0.14)	100.23	(0.14)	99.95	(-0.03)	99.98	(-0.01)
S2	99.65	(-0.90)	99.95	(-0.14)	99.60	(-1.06)	99.90	(-0.26)
HCN	99.94	(-0.15)	99.99	(-0.03)	99.88	(-0.31)	99.94	(-0.16)
C2H2	99.94	(-0.13)	99.99	(-0.03)	99.90	(-0.23)	99.94	(-0.14)
RMSD:		(0.44)		(0.15)		(0.53)		(0.25)
Max:		(-1.22)		(0.47)		(-1.37)		(-0.78)

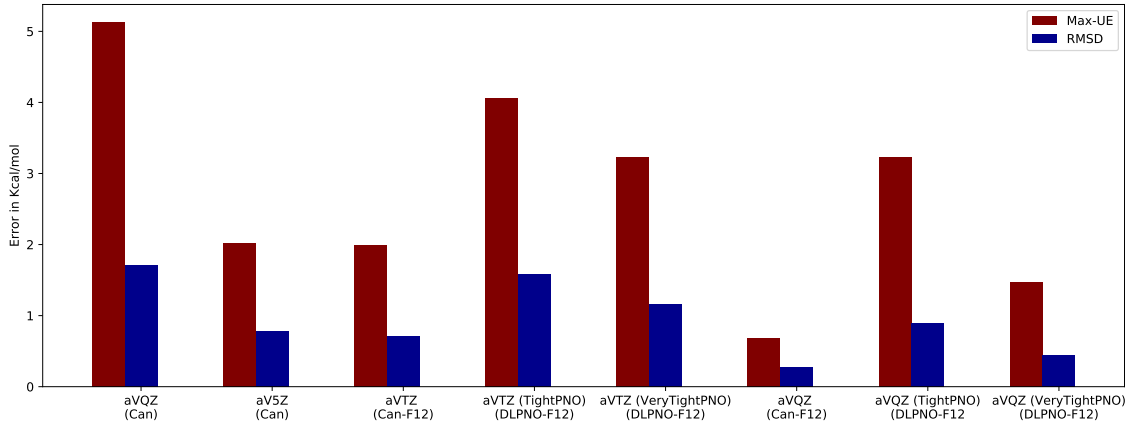


FIG. 4: Max unsigned error and RMSD in kcal/mol in the reaction energies of the test set for the canonical CCSD(T) (Can), CCSD(T) $_{\overline{\text{F12}}}$ (Can-F12) and DLPNO-CCSD(T) $_{\overline{\text{F12}}}$ (DLPNO-F12) methods with respect to the CBS values.

to the canonical CCSD(T) $_{\overline{\text{F12}}}$ values, where the numbers in the parentheses denote the errors in kcal/mol. For the aVTZ basis, the RMSD and max errors for **TightPNO** and **VeryTightPNO** settings are (0.44,-1.22) and (0.15,0.47) kcal/mol while for the aVQZ basis, the errors come out to be (0.53,-1.37) and (0.25,-0.78) kcal/mol respectively. Fig. 4 illustrates the max unsigned error and RMSD of REs of the test set for the canonical CCSD(T) (Can), CCSD(T) $_{\overline{\text{F12}}}$ (Can-F12) and CCSD(T) $_{\overline{\text{F12}}}$ (DLPNO-F12) methods with respect to the CBS values. The basis set limit was estimated by using the Helgaker’s two point extrapolation formula[115] using aVQZ and aV5Z canonical CCSD(T) correlation energies. The HF energy and the direct singles term ($F_{at_i}^{i_a}$) was taken from the larger basis set. The Can-F12 method with aVTZ basis set is seen to perform slightly better than its conventional counterpart with aV5Z basis set: (0.72,1.99) vs (0.79,2.03) kcal/mol. However, these errors are far from satisfactory and reflect the highly sensitive nature of these REs to the basis set size. For the same test set, Werner reported improved results of (0.53,1.34) kcal/mol with his iterative CCSD(T)-F12b/aVTZ approach which usually gives very similar results to our CCSD(T) $_{\overline{\text{F12}}}$ method for closed-shell systems[108]. The DLPNO-F12 method on the other hand resulted in quite large errors for the same basis set: (1.58,4.06) for **TightPNO** and (1.16,3.23) kcal/mol for **VeryTightPNO** settings. Thus, the aVTZ basis set is unable to provide the desired accuracy with both canonical and DLPNO-F12 methods. Finally, the Can-F12 method with aVQZ basis set reduces the errors further to (0.27,0.68) kcal/mol

while the DLPNO approximations yield errors of (0.89,3.23) and (0.44,1.47) kcal/mol with `TightPNO` and `VeryTightPNO` settings respectively. Werner on the other hand obtained errors of (0.20,0.50) kcal/mol with the CCSD(T)-F12b/aVQZ method[108].

This relatively poor performance of the DLPNO approach can be attributed to the PNOs being a suboptimal representation for capturing the F12 correlation effects. This is specially true for the PNOs of SOMO-DOMO pairs, for example, for the C atom in the aVTZ basis 10 PNOs contribute as much as 12% of the F12 correlation energy for the SOMO-DOMO pairs in spite of having zero pair-density eigenvalue and having almost negligible contribution to the DLPNO-CCSD(T) correlation energy (This will be elaborated in more detail in our future work). Furthermore, the errors in REs are further amplified by the lack of intrinsic error cancellations as the DLPNO-CCSD(T) $_{\overline{\text{F12}}}$ correlation energies of closed shell and most of the open shell species approach towards the canonical limit from above (<100%) and below respectively (see Table I). This primarily happens due to the overestimation of the F12 correlation energy for the SOMO-DOMO pairs in the truncated PNO basis. The errors in REs are thus the largest for the smaller systems where the SOMO-DOMO F12 correlation energies constitute a significant portion of the total F12 correction and hence a bigger basis set like aVQZ with `VeryTightPNO` truncation parameters is required for a favorable comparison with the CBS values for such systems. We also plan to employ open-shell geminal spanning orbitals (GSOs), earlier proposed by some of us[93] within the DLPNO framework as an alternative to PNOs in order to cut down the computational costs associated with the `VeryTightPNO` truncation settings.

C. Computational scaling

In this section, we analyze the scaling behavior of both DLPNO-CCSD(T) and DLPNO-CCSD(T) $_{\overline{\text{F12}}}$ methods for open-shell systems, while employing the less expensive T0 variant of (T) (due to the compute time constraints) although similar trends are expected to hold for the rigorous (T1) variant as well. We have chosen the perturbative triples method (instead of just CCSD) as well in this analysis as the F12 correction is often used in conjunction with the CCSD(T) procedure. Fig. 5 shows the wall clock time in seconds for both UHF-DLPNO-CCSD(T) and UHF-DLPNO-CCSD(T) $_{\overline{\text{F12}}}$ calculations on quasilinear n-alkane chains C_nH_{2n+2} in triplet state, from $n=120$ to $n=160$. These calculations utilized

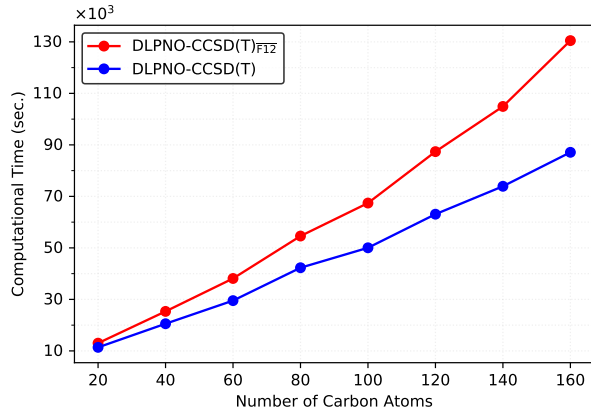
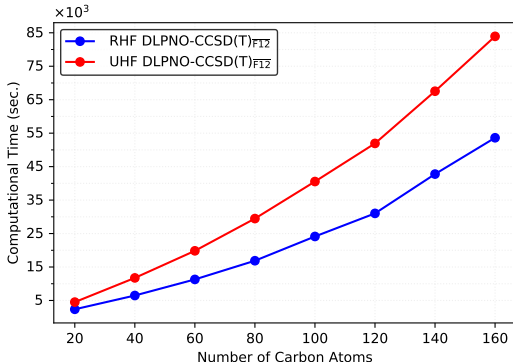


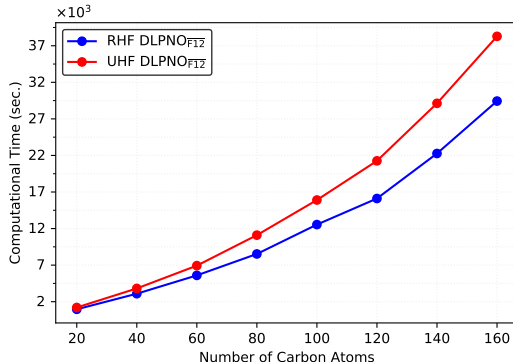
FIG. 5: Wall clock time in seconds for UHF-DLPNO-CCSD(T) and UHF-DLPNO-CCSD(T)_{F12} correlation energy calculations with `TightPNO` settings on quasilinear n-alkane chains C_nH_{2n+2} , in triplet state from $n=20$ to $n=160$. Following basis set quartet were used: {def2-TZVP, def2-TZVP/RI, cc-pVDZ-F12-OptRI, def2/J} {OBS, DFBS, CABS, CDFBS} and the COSX procedure for evaluating the exchange operator was employed. All these calculations utilized 4 CPU cores (4 MPI processes) and a total of 512 GB memory.

4 CPU cores (4 MPI processes) and a total of 512 GB memory. The effective exponents for the UHF-DLPNO-CCSD(T) and UHF-DLPNO-CCSD(T)_{F12} calculations from Fig. 5 came out to be **1.06** and **1.23** respectively. The deviation from linear scaling for the UHF-DLPNO-CCSD(T)_{F12} method can be attributed to almost quadratic scaling 1-external RI integral generation in the crude guess step[56] and the cubically scaling density fitted evaluation of the Coulomb operator (\hat{J}) in OBS (O) and CABS (C) spaces: \hat{J}_{OO} , \hat{J}_{CO} and \hat{J}_{CC} . Furthermore, some of the I/O steps in the pair-specific PNO integral generation procedure in F12 (which number as $2 \times N_{\text{Pairs}}$) doesn't scale linearly as we go to more than 100 atoms. We hope to address these terms in the near future. In $C_{160}H_{322}$, the time spent in F12 procedure is mostly divided into 3 parts: 3-index RI integral transformation to PAO basis (39%), the Fock matrix construction (27%) and the evaluation of intermediates in PNO basis(31%) (refer to TableII) and the entire F12 procedure took about 33% of the total computational time. We also looked at the scaling behavior of our method for a series of triplet $[(C_4SH_3) - (CH_2)_N - (C_4SH_3)^{2+}]$ diradical molecules (with $N=0..50$) previously used to study computational scaling with the system size[42] using identical settings as above (refer to the Supporting Information for the corresponding plot). We also compared both RHF

and UHF variants of $\text{DLPNO-CCSD(T)}_{\overline{\text{F12}}}$ for n-alkanes as above in the singlet state. The



(a) RHF/UHF $\text{DLPNO-CCSD(T)}_{\overline{\text{F12}}}$



(b) RHF/UHF DLPNO-F12

FIG. 6: a) Total and b) F12-only computation time (in seconds) for closed- and open-shell $\text{DLPNO-CCSD(T)}_{\overline{\text{F12}}}$ implementations with `TightPNO` settings on quasilinear n-alkane chains $\text{C}_n\text{H}_{2n+2}$, in singlet state from $n=20$ to $n=160$. Following basis set quartet were used: {def2-TZVP, def2-TZVP/RI, cc-pVDZ-F12-OptRI, def2/J} {OBS, DFBS, CABS, CDFBS} and the COSX procedure for evaluating the exchange operator was employed. All these calculations utilized 4 CPU cores (4 MPI processes) and a total of 512 GB memory.

correlation energies obtained from both closed- and open-shell $\text{DLPNO-CCSD(T)}_{\overline{\text{F12}}}$ methods match up to 5 decimal points, signifying balanced treatment of open- and closed-shell systems by our approach. From Fig. 6a and Fig. 6b, it can be seen that the UHF code is only fractionally more expensive than the RHF code. Specifically, for $\text{C}_{160}\text{H}_{322}$ alkane, the UHF- DLPNO-CCSD(T) method is only 1.5 times its closed shell counterpart even though the CCSD iterations in the open-shell could be 3-4 times more expensive due to the appearance of more pairs $(\alpha-\alpha, \alpha-\beta, \beta-\beta)$. Furthermore, if we look at only the F12 part of calculations (Fig. 6b), the difference is even smaller and the UHF code is only expensive 1.3 times for the same alkane, helped by the fact that one doesn't need to solve 3-sets of CC amplitude-like equations in the F12 part. For a small number of SOMOs, both integral transformations and evaluation of F12 intermediates is only marginally expensive (compared to closed-shell) in the open-shell case. Of course, additional (spin) evaluations of the exchange operator in different spaces are required. A favorable comparison with the closed-shell code makes this a successful extension of the $\text{RHF-DLPNO-CCSD(T)}_{\overline{\text{F12}}}$ formalism to open-shell systems.

D. Medium and large molecules

In this section, we analyze the timings of sample UHF-DLPNO-CCSD(T)_{F12} calculations on representative medium-sized and large molecular species which are currently beyond the reach of the corresponding canonical formalisms. Their optimized geometries were taken from the SI of Ref[56]. Dioxygenate, Vitamine E succinate, Cochineal Carmine and Hexanitrohexaazaisowurtzitane (CL20) constitutes our set of medium sized molecules. Both the transition-state (*ts*) and educt models of of the dioxygenase enzyme active site[116] are considered. Model compounds for the active center of the [NiFe] hydrogenase enzyme[117] (triplet state) and bicarbonate in Photosystem II[118] were chosen as test-cases for assessing the performance of the UHF-DLPNO-CCSD(T)_{F12} method for larger systems. For all the transition metal complexes, QROs obtained from open-shell density functional calculations with CAM-B3LYP functional[119] were used as reference orbitals. Furthermore, the RIJCOSX approximation (using def2/J as CDFBS) was used to evaluate the Fock matrix. Since optimized CABS basis sets are not available for transition metals like Fe and Ni, the *uncontracted* def2-TZVPP (bicarbonate) and def2-QZVPP (dioxygenate, [NiFe] hydrogenase) basis sets were used as the CABS. While, medium-sized molecular calculations used the `TightPNO` truncation settings, `NormalPNO` settings were used for the bigger calculations. Also, the semi-canonical non-iterative (T0) variant of the (T) procedure was employed. All calculations utilized 4 CPU cores (4 MPI processes) and 512GB memory. Table II shows the breakdown of wall time (in seconds) for different (prominent) computational steps involved in the UHF-DLPNO-CCSD(T)_{F12} procedure excluding the preceding reference calculations. Timings of C₁₆₀H₃₂₂ molecule has also been added for comparison purposes. It can be seen that the time spent in the F12 procedure for the medium sized molecules is only a tiny fraction of the total execution time and ranges from 3.8% in educt dioxygenate to 12.7% in Vitamin E succinate. For the C₁₆₀H₃₂₂ molecule, however, the F12 contribution is a bit higher at 33.2% because of the comparatively faster (T) calculation. For the larger systems, only DLPNO-CCSD_{F12} calculations were carried out and the time spent in the F12 part come out to be 39.8% and 40.2% for Bicarbonate and [NiFe] hydrogenase molecules respectively. Obviously, this will be lowered significantly if the (T) correction was included (especially, the iterative (T1) variety), as it would normally be for practical applications that call for the high-precision provided by the explicitly-correlated coupled-cluster. The F12 correction

for the Bicarbonate system took around 26 hours, and is the most extensive F12 calculation reported in this work, including more than 500 atoms. Thus clearly very large systems can be already treated by the presented open-shell DLPNO-CCSD(T) $_{\overline{\text{F12}}}$ approach. However there is additional untapped potential for optimization in our implementation, besides obvious ones (like large-scale parallelization). Inside the F12 part of the calculation, a significant portion of time is spent in the Fock matrix formation, integral transformations in the PAO space, calculation of pair-specific CABS space, pair-specific OBS/OBS and CABS/OBS integral generations in PNO basis and the evaluation of the \bar{V} intermediate. As mentioned before, the I/O in the OBS/OBS and CABS/OBS integral generation routine can still be brought down significantly. Currently, the pair-extended integrals in the PAO space are read from disk for every occupied orbital i and j appearing in the F12 pair list, resulting in a $2 \times N_{\text{Pairs}}$ I/O operations, followed by integral sieving to extract only the i and j specific integrals which are then finally fused to construct the integrals associated with the ij pair. This could be changed into a having a loop over occupied orbitals i , and then generating all the OBS/OBS and CABS/OBS integrals for all the j orbitals connected to the orbital i . This way, the number of I/O steps would be reduced to the number of occupied orbitals, which in principle, should lower down the prefactor of the PNO integral generation part of the code significantly. Also, similar to the works of Tew et al.[77], the generation of the CABS space could be made cheaper by making use of a more compact representation for the CABS orbitals like OSVs than just the regular AOs.

These optimizations will be pursued further in future work.

TABLE II: Computational timings (in seconds) for the various steps of the DLPNO-CCSD(T)_{F12} procedure along with reference, correlation and F12 correction energies for representative medium-sized and large open-shell systems. Reference calculations on all molecules (except C₁₆₀H₃₂₂) were done using UKS/CAM-B3LYP. RIJCOSX approximation was used in all these calculations (using def2/J basis set) and each calculation utilized 4 CPU cores (4 MPI processes) and a total of 512 GB memory.

	Dioxygenate (ts)[72]	Dioxygenate (educt)[72]	Vitamin E[111]	Cochineal[111]	CL20[111]	C ₁₆₀ H ₃₂₂ [120]	Bicarbonate[121]	[NiFe] hydrogenase[122]
Total execution time:	17318	19344	60724	130252	234992	130492	239032	130505
Time in CCSD procedure:	8594	10996	22006	40985	82225	68081	143888	78000
Time in (T) procedure:	7979	7611	31002	78122	142888	19031	-	-
Total time and % in F12 procedure:	744 (4.3%)	736 (3.8%)	7716 (12.7%)	11144 (8.6%)	9878 (4.2%)	43380 (33.2%)	95144 (39.8%)	52504 (40.2%)
Fock matrix formation	50	50	504	406	245	11776	12513	4026
Integral transformations (PAO)	141	141	2596	2208	1122	16897	67788	26531
Pair-specific 1e matrix	24	24	505	875	706	872	1614	2505
Local fit metric generation	35	33	120	270	309	68	91	310
Calculation of CABS	32	32	668	1144	818	1951	3097	3295
OBS/OBS integral generation	30	30	218	380	372	1570	748	1441
CABS/OBS integral generation	84	84	938	1512	1386	3346	5237	4754
V_{ij}, fX_{ij}, B_{ij} Intermediates	16	17	156	303	332	263	790	748
\tilde{V}_{ij} Intermediate	292	287	1808	3606	4202	1631	1950	7932
Reference energy:	-1940.059567	-1940.064296	-1276.512050	-1818.281941	-1781.258625	-6248.368368	-15181.158996	-7843.018084
F12 correction to reference energy:	-0.037876	-0.037977	-0.076530	-0.102759	-0.111546	-0.357284	-11.205403	-0.163318
CCSD Correlation energy:	-3.068416	-3.068244	-5.480703	-6.370557	-6.035779	-28.781440	-46.386367	-17.248012
F12 correction to CCSD correction energy:	-0.314036	-0.314318	-0.610031	-0.838685	-0.783082	-2.326865	-11.221550	-1.321897
(T) correlation energy:	-0.135943	-0.133316	-0.243998	-0.309254	-0.340798	-1.125222	-	-
Total energy:	-1943.615838	-1943.616152	-1282.923311	-1825.903196	-1788.529831	-6280.959179	-15249.972316	-7861.751311
no. of SOMOs:	6	6	1	1	1	2	4	2
no. of atoms:	22	22	80	55	36	482	565	180
size of AO basis:	545	545	1371	1230	954	6892	5420	4007
size of DF basis:	1352	1352	3359	2980	2298	16990	17743	9594
size of CABS basis[123]	1351	1351	4872	4335	3348	27426	17702	9810

V. CONCLUSION

We have developed a robust explicitly correlated DLPNO-CCSD(T)_{F12} method for high-spin open-shell species whose costs and storage scale nearly linearly with the system size. For representative applications we found that the time spent inside the F12 part of the calculations is only a fraction of the total computation time. We were able to carry out F12 calculations on the model compound of bicarbonate present in the PSII enzyme, which involved over 5000 basis-functions and more than 500 atoms, which to our knowledge, is the most extensive open-shell F12 calculation to this date.

The approach allows to compute CCSD(T) energies that approach the complete basis set limit very closely. For example, when using only a aug-cc-pVTZ basis set and the `TightPNO` truncation settings (default for F12) the DLPNO-CCSD(T)_{F12} heats of formation of 50 largest molecules out of the ANL database of 348 core combustion species are within 0.4 kcal/mol of the reference extrapolated CBS CCSD(T) values. The deviation is further lowered to ≈ 0.3 kcal/mol with extrapolation of DLPNO-CCSD(T)_{F12} results with aug-cc-pVDZ and aug-cc-pVTZ basis sets. We also examined the reaction energies of 50 open-shell reactions with large reaction energies and strong basis set dependence where we obtained a RMSD of ~ 0.4 kcal/mol with the aug-cc-pVQ(+d)Z basis set. However, `VeryTightPNO` truncation settings were employed for these calculations resulting in a significant increase in the associated computational costs. The use of open-shell GSOs[93] will be explored in our next work as an alternative to PNOs as they have been shown to be much more compact for describing F12 intermediates. Thus, the DLPNO-CCSD(T)_{F12} method is an attractive alternative to purely extrapolation based canonical and reduced-scaling CCSD(T) formalisms. The F12/D approximation[79] (used in all the F12 calculations reported in the paper), which avoids the need for explicit evaluation of the exchange operator in the CABS-CABS space and is hence computationally cheaper, is recommended along with the `TightPNO` truncation settings. A production-quality implementation of the DLPNO-CCSD(T)_{F12} method has been implemented in the 4.2 version of the ORCA quantum chemistry package, making it suitable for a widespread use in the chemistry community. Further improvements in the DLPNO F12 code like the introduction of GSOs[93], compact representation of the CABS space, and reduction of I/O steps in the evaluation of intermediates are expected in the near future.

SUPPLEMENTARY MATERIAL

See supplementary material for a) individual heats of formation of the 50 largest molecules of the ANL database and b) the scaling plot of the DLPNO-CCSD(T)_{F12} method for a series of triplet [(C₄SH₃) – (CH₂)_N – (C₄SH₃)²⁺] diradical molecules.

ACKNOWLEDGMENTS

This work was supported by the U.S. National Science Foundation (awards 1550456 and 1800348) and by the Exascale Computing Project (17-SC-20-SC), a collaborative effort of the U.S. Department of Energy Office of Science and the National Nuclear Security Administration. The authors acknowledge Virginia Tech’s Advanced Research Computing center (ARC) for providing computational resources and technical support that made this work possible.

Data Availability Statement

The data that supports the findings of this study are available within the article and its supplementary material while the (remaining) raw data are available from the corresponding author upon request.

-
- [1] K. Raghavachari, G. W. Trucks, J. A. Pople, and M. Head-Gordon, “A fifth-order perturbation comparison of electron correlation,” *Chem. Phys. Lett.* **157**, 479 (1989).
 - [2] O. Sinanoğlu, “Many-Electron Theory of Atoms, Molecules and Their Interactions,” *Adv. Chem. Phys.* **6**, 315 (1964).
 - [3] R. K. Nesbet, “Electronic Correlation in Atoms and Molecules,” *Adv. Chem. Phys.* **9**, 321 (1965).
 - [4] P. Pulay, “Localizability of dynamic electron correlation,” *Chem. Phys. Lett.* **100**, 151–154 (1983).
 - [5] S. Saebø and P. Pulay, “Fourth-order Møller-Plesset perturbation theory in the local correlation treatment. I. Method,” *J. Chem. Phys.* **86**, 914–922 (1986).

- [6] S. Saebø and P. Pulay, “Local treatment of electron correlation,” *Annu. Rev. Phys. Chem.* **44**, 213–236 (1993).
- [7] M. Schütz, G. Hetzer, and H.-J. Werner, “Linear scaling local electron correlation methods. I. Linear scaling local MP2,” *J. Chem. Phys.* **111**, 5691–5705 (1999).
- [8] G. Hetzer, M. Schütz, H. Stoll, and H.-J. Werner, “Low-order scaling local correlation methods. II: Splitting the Coulomb operator in linear scaling local second-order Møller-Plesset perturbation theory,” *J. Chem. Phys.* **113**, 9443–9455 (2000).
- [9] M. Schütz, “Low-order scaling local electron correlation methods. III. Linear scaling local perturbative triples correction (T),” *J. Chem. Phys.* **113**, 9986–10001 (2000).
- [10] M. Schütz and H.-J. Werner, “Low-order scaling local correlation methods. IV. Linear scaling local coupled-cluster (LCCSD),” *J. Chem. Phys.* **114**, 661–681 (2001).
- [11] M. Schütz, “Low-order scaling local electron correlation methods. V. Connected triples beyond (T): Linear scaling local CCSDT-1b,” *J. Chem. Phys.* **116**, 8772–8785 (2002).
- [12] C. Riplinger, B. Sandhoefer, A. Hansen, and F. Neese, “Natural triple excitations in local coupled cluster calculations with pair natural orbitals.” *J. Chem. Phys.* **139**, 134101 (2013).
- [13] P. Pinski, C. Riplinger, E. F. Valeev, and F. Neese, “Sparse maps—A systematic infrastructure for reduced-scaling electronic structure methods. I. An efficient and simple linear scaling local MP2 method that uses an intermediate basis of pair natural orbitals,” *J. Chem. Phys.* **143**, 034108 (2015).
- [14] H.-J. Werner, G. Knizia, C. Krause, M. Schwilk, and M. Dornbach, “Scalable Electron Correlation Methods I.: PNO-LMP2 with Linear Scaling in the Molecular Size and Near-Inverse-Linear Scaling in the Number of Processors,” *J. Chem. Theory Comput.* **11**, 484–507 (2015).
- [15] H. R. McAlexander and T. D. Crawford, “A Comparison of Three Approaches to the Reduced-Scaling Coupled Cluster Treatment of Non-Resonant Molecular Response Properties,” *J. Chem. Theory Comp.* **12**, 209–222 (2016).
- [16] C. Edmiston and M. Krauss, “Pseudonatural Orbitals as a Basis for the Superposition of Configurations. I. He_2^+ ,” *J. Chem. Phys.* **45**, 1833–1839 (1966).
- [17] W. Meyer, “PNO-CI Studies of Electron Correlation Effects. I. Configuration Expansion by Means of Nonorthogonal Orbitals, and Application of the Ground State and Ionized States of Methane,” *J. Chem. Phys.* **58**, 1017 (1973).

- [18] W. Meyer, "Pno-ci and cepa studies of electron correlation effects," *Theor. Chim. Acta* **35**, 277–292 (1974).
- [19] R. Ahlrichs, H. Lischka, V. Staemmler, and W. Kutzelnigg, "PNO-CI (Pair Natural Orbital Configuration Interaction) and CEPA-PNO (Coupled Cluster Pair Approximation with Pair Natural Orbitals) Calculations of Molecular Systems. I. Outline of the Method for Closed-Shell States," *J. Chem. Phys.* **62**, 1225–1234 (1975).
- [20] F. Neese, F. Wennmohs, and A. Hansen, "Efficient and accurate local approximations to coupled-electron pair approaches: An attempt to revive the pair natural orbital method," *The Journal of Chemical Physics* **130**, 114108 (2009), <https://doi.org/10.1063/1.3086717>.
- [21] F. Neese, A. Hansen, and D. G. Liakos, "Efficient and accurate approximations to the local coupled cluster singles doubles method using a truncated pair natural orbital basis," *J. Chem. Phys.* **131**, 064103 (2009).
- [22] C. Riplinger and F. Neese, "An efficient and near linear scaling pair natural orbital based local coupled cluster method." *J. Chem. Phys.* **138**, 034106 (2013).
- [23] C. Riplinger, P. Pinski, U. Becker, E. F. Valeev, and F. Neese, "Sparse maps—A systematic infrastructure for reduced-scaling electronic structure methods. II. Linear scaling domain based pair natural orbital coupled cluster theory," *J. Chem. Phys.* **144**, 024109 (2016), <https://doi.org/10.1063/1.4939030>.
- [24] Q. Ma and H.-J. Werner, "Scalable electron correlation methods. 2. parallel PNO-LMP2-F12 with near linear scaling in the molecular size," *J. Chem. Theory Comput.* **11**, 5291–5304 (2015).
- [25] D. P. Tew, B. Helmich, and C. Hättig, "Local explicitly correlated second-order Møller–Plesset perturbation theory with pair natural orbitals," *J. Chem. Phys.* **135**, 074107 (2011), <https://doi.org/10.1063/1.3624370>.
- [26] C. Hättig, D. P. Tew, and B. Helmich, "Local explicitly correlated second- and third-order Møller–Plesset perturbation theory with pair natural orbitals," *J. Chem. Phys.* **136**, 204105 (2012), <https://doi.org/10.1063/1.4719981>.
- [27] M. S. Frank, G. Schmitz, and C. Hättig, "The PNO–MP2 gradient and its application to molecular geometry optimisations," *Mol. Phys.* **115**, 343–356 (2017), <https://doi.org/10.1080/00268976.2016.1263762>.
- [28] P. Pinski and F. Neese, "Analytical gradient for the domain-based local pair natural orbital

- second order Møller-Plesset perturbation theory method (DLPNO-MP2),” *J. Chem. Phys.* **150**, 164102 (2019), <https://doi.org/10.1063/1.5086544>.
- [29] B. Helmich and C. Hättig, “A pair natural orbital implementation of the coupled cluster model CC2 for excitation energies,” *J. Chem. Phys.* **139**, 084114–084114–13 (2013).
- [30] B. Helmich and C. Hättig, “A pair natural orbital based implementation of ADC(2)-x: Perspectives and challenges for response methods for singly and doubly excited states in large molecules,” *Comput. Theor. Chem.* **1040-1041**, 35–44 (2014).
- [31] M. S. Frank and C. Hättig, “A pair natural orbital based implementation of CCSD excitation energies within the framework of linear response theory,” *J. Chem. Phys.* **148**, 134102 (2018), <https://doi.org/10.1063/1.5018514>.
- [32] A. Kumar Dutta, M. Nooijen, F. Neese, and R. Izsák, “Exploring the Accuracy of a Low Scaling Similarity Transformed Equation of Motion Method for Vertical Excitation Energies,” *J. Chem. Theory Comput.* **14**, 72–91 (2017).
- [33] D. Mester, P. R. Nagy, and M. Kállay, “Reduced-Scaling Correlation Methods for the Excited States of Large Molecules: Implementation and Benchmarks for the Second-Order Algebraic-Diagrammatic Construction Approach,” *J. Chem. Theory Comput.* **15**, 6111–6126 (2019), pMID: 31553611, <https://doi.org/10.1021/acs.jctc.9b00735>.
- [34] A. Dittmer, R. Izsák, F. Neese, and D. Maganas, “Accurate Band Gap Predictions of Semiconductors in the Framework of the Similarity Transformed Equation of Motion Coupled Cluster Theory,” *Inorg. Chem.* **58**, 9303–9315 (2019).
- [35] C. A. M. Salla, J. dos Santos, G. Farias, A. J. Bortoluzzi, S. F. Curcio, T. Cazati, R. Izsák, F. Neese, B. de Souza, and I. H. Bechtold, “New Boron(III) Blue Emitters for All-Solution Processed OLEDs: Molecular Design Assisted by Theoretical Modeling,” *Eur. J. Inorg. Chem.* **2019**, 2247–2257 (2019).
- [36] A. K. Dutta, M. Saitow, C. Riplinger, F. Neese, and R. Izsák, “A near-linear scaling equation of motion coupled cluster method for ionized states,” *J. Chem. Phys.* **148**, 244101 (2018), <https://doi.org/10.1063/1.5029470>.
- [37] A. K. Dutta, M. Saitow, B. Demoulin, F. Neese, and R. Izsák, “A domain-based local pair natural orbital implementation of the equation of motion coupled cluster method for electron attached states,” *J. Chem. Phys.* **150**, 164123 (2019), <https://doi.org/10.1063/1.5089637>.
- [38] S. Haldar, C. Riplinger, B. Demoulin, F. Neese, R. Izsák, and A. K. Dutta, “Mul-

- tilayer Approach to the IP-EOM-DLPNO-CCSD Method: Theory, Implementation, and Application,” *J. Chem. Theory Comput.* **15**, 2265–2277 (2019), pMID: 30860835, <https://doi.org/10.1021/acs.jctc.8b01263>.
- [39] T. D. Crawford, A. Kumar, A. P. Bazanté, and R. Di Remigio, “Reduced-scaling coupled cluster response theory: Challenges and opportunities,” *WIREs Comput. Mol. Sci.* **9**, e1406 (2019), <https://onlinelibrary.wiley.com/doi/pdf/10.1002/wcms.1406>.
- [40] O. Demel, J. Pittner, and F. Neese, “A Local Pair Natural Orbital-Based Multireference Mukherjee’s Coupled Cluster Method,” *J. Chem. Theory Comput.* **11**, 3104–3114 (2015), pMID: 26575747, <https://doi.org/10.1021/acs.jctc.5b00334>.
- [41] F. Menezes, D. Kats, and H.-J. Werner, “Local complete active space second-order perturbation theory using pair natural orbitals (PNO-CASPT2),” *J. Chem. Phys.* **145**, 124115 (2016), <https://doi.org/10.1063/1.4963019>.
- [42] Y. Guo, K. Sivalingam, E. F. Valeev, and F. Neese, “SparseMaps—A systematic infrastructure for reduced-scaling electronic structure methods. III. Linear-scaling multireference domain-based pair natural orbital N-electron valence perturbation theory,” *J. Chem. Phys.* **144**, 094111 (2016), <https://doi.org/10.1063/1.4942769>.
- [43] J. Brabec, J. Lang, M. Saitow, J. Pittner, F. Neese, and O. Demel, “Domain-Based Local Pair Natural Orbital Version of Mukherjee’s State-Specific Coupled Cluster Method,” *J. Chem. Theory Comput.* **14**, 1370–1382 (2018), pMID: 29345924, <https://doi.org/10.1021/acs.jctc.7b01184>.
- [44] I. G. D. Purvis and R. J. Bartlett, “A full coupled-cluster singles and doubles model: The inclusion of disconnected triples,” *J. Chem. Phys.* **76**, 1910–1918 (1982).
- [45] M. Rittby and R. J. Bartlett, “An open-shell spin-restricted coupled cluster method: Application to ionization potentials in N₂,” *J. Phys. Chem.* **92**, 3033–3036 (1988).
- [46] J. D. Watts and R. J. Bartlett, “The coupled-cluster single, double and triple excitation model for open-shell single reference functions,” *J. Chem. Phys.* **93**, 6104–6105 (1990).
- [47] C. L. Janssen and H. F. Schaefer, III, “The automated solution of second quantization equations with applications to the coupled cluster approach,” *Theoretical Chemistry* **79**, 1–42 (1991).
- [48] J. G. J. D. Watts and R. J. Bartlett, “Coupled-cluster methods with noniterative triple excitations for restricted open-shell Hartree-Fock and other general single determinant reference

- functions. Energies and analytical gradients,” *J. Chem. Phys.* **98**, 8718–8733 (1993).
- [49] X. Li and J. Paldus, “Automation of the implementation of spin-adapted open-shell coupled-cluster theories relying on the unitary group formalism,” *J Chem Phys* **101**, 8812–8826 (1994).
- [50] R. J. Bartlett and M. Musial, “Coupled-cluster theory in quantum chemistry,” *Revs. of Modern Phys.* **79**, 291–352 (2007).
- [51] A. I. Krylov, “Equation-of-Motion Coupled-Cluster Methods for Open-Shell and Electronically Excited Species: The Hitchhiker’s Guide to Fock Space,” *Annu. Rev. Phys. Chem.* **59**, 433–462 (2008).
- [52] R. J. Bartlett, “The coupled-cluster revolution,” *Molecular Physics* **108**, 2905–2920 (2010), <https://doi.org/10.1080/00268976.2010.531773>.
- [53] R. J. Bartlett, “Coupled-cluster theory and its equation-of-motion extensions,” *WIREs Computational Molecular Science* **2**, 126–138 (2012), <https://onlinelibrary.wiley.com/doi/pdf/10.1002/wcms.76>.
- [54] F. Neese, “Importance of Direct Spin-Spin Coupling and Spin-Flip Excitations for the Zero-Field Splittings of Transition Metal Complexes: A Case Study,” *J. Am. Chem. Soc* **128**, 10213–10222 (2006), pMID: 16881651, <https://doi.org/10.1021/ja061798a>.
- [55] A. Hansen, D. G. Liakos, and F. Neese, “Efficient and accurate local single reference correlation methods for high-spin open-shell molecules using pair natural orbitals,” *J. Chem. Phys.* **135**, 214102 (2011), <https://doi.org/10.1063/1.3663855>.
- [56] M. Saitow, U. Becker, C. Riplinger, E. F. Valeev, and F. Neese, “A new near-linear scaling, efficient and accurate, open-shell domain-based local pair natural orbital coupled cluster singles and doubles theory,” *J. Chem. Phys.* **146**, 164105 (2017).
- [57] Y. Guo, C. Riplinger, D. G. Liakos, U. Becker, M. Saitow, and F. Neese, “Linear scaling perturbative triples correction approximations for open-shell domain-based local pair natural orbital coupled cluster singles and doubles theory [DLPNO-CCSD(T0/T)],” *J. Chem. Phys.* **152**, 024116 (2020), <https://doi.org/10.1063/1.5127550>.
- [58] C. Krause and H.-J. Werner, “Scalable Electron Correlation Methods. 6. Local Spin-Restricted Open-Shell Second-Order Møller–Plesset Perturbation Theory Using Pair Natural Orbitals: PNO-RMP2,” *J. Chem. Phys.* **15**, 987–1005 (2019), <https://doi.org/10.1021/acs.jctc.8b01012>.
- [59] Q. Ma and H.-J. Werner, “Scalable Electron Correlation Methods. 7. Local Open-Shell Coupled-Cluster Methods Using Pair Natural Orbitals: PNO-RCCSD and PNO-UCCSD,”

- J. Chem. Theory Comput. (2020).
- [60] W. Kutzelnigg and J. D. Morgan, "Rates of convergence of the partial-wave expansions of atomic correlation energies," J. Chem. Phys. **96**, 4484 (1992).
- [61] W. Kutzelnigg, " r_{12} -Dependent terms in the wave function as closed sums of partial wave amplitudes for large l ," Theor. Chim. Acta **68**, 445–469 (1985).
- [62] W. Klopper and C. C. Samson, "Explicitly correlated second-order Møller–Plesset methods with auxiliary basis sets," J. Chem. Phys. **116**, 6397–6410 (2002).
- [63] F. R. Manby, "Density fitting in second-order linear- r_{12} Møller–Plesset perturbation theory," J. Chem. Phys. **119**, 4607 (2003).
- [64] S. Ten-no, "Explicitly correlated second order perturbation theory: introduction of a rational generator and numerical quadratures." J. Chem. Phys. **121**, 117–29 (2004).
- [65] S. Ten-no, "*Initiation of explicitly correlated Slater-type geminal theory*," Chem. Phys. Lett. **398**, 56–61 (2004).
- [66] E. F. Valeev, "Improving on the resolution of the identity in linear R12 ab initio theories," Chem. Phys. Lett. **395**, 190–195 (2004).
- [67] S. Kedžuch, M. Milko, and J. Noga, "Alternative formulation of the matrix elements in MP2-R12 theory," Int. J. Quantum Chem. **105**, 929–936 (2005).
- [68] H. Fliegl, W. Klopper, and C. Hättig, "Coupled-cluster theory with simplified linear- r_{12} corrections: The CCSD (R12) model," J. Chem. Phys. (2005).
- [69] H. J. Werner, T. B. Adler, and F. R. Manby, "General orbital invariant MP2-F12 theory," J. Chem. Phys. **126**, 164102 (2007).
- [70] E. F. Valeev, "Coupled-cluster methods with perturbative inclusion of explicitly correlated terms: a preliminary investigation," Phys. Chem. Chem. Phys. **10**, 106–113 (2008).
- [71] J. Zhang and E. F. Valeev, "Prediction of Reaction Barriers and Thermochemical Properties with Explicitly Correlated Coupled-Cluster Methods: A Basis Set Assessment," J. Chem. Theory Comput. **8**, 3175–3186 (2012).
- [72] However, further numerical approximations like the resolution of identity in the F12 methods can sometimes slow down this convergence. Furthermore, precise analysis of the basis set convergence of correlation energy for molecules is more phenomenological than for atoms.
- [73] D. G. Liakos, R. Izsák, E. F. Valeev, and F. Neese, "What is the most efficient way to reach the canonical MP2 basis set limit?" Mol. Phys. **111**, 2653–2662 (2013),

<https://doi.org/10.1080/00268976.2013.824624>.

- [74] J. Yang, G. K.-L. Chan, F. R. Manby, M. Schütz, and H.-J. Werner, “The orbital-specific-virtual local coupled cluster singles and doubles method,” *J. Chem. Phys.* **136**, 144105–144105–16 (2012).
- [75] C. Krause and H.-J. Werner, “Comparison of explicitly correlated local coupled-cluster methods with various choices of virtual orbitals.” *Phys. Chem. Chem. Phys.* **14**, 7591–7604 (2012).
- [76] D. P. Tew and C. Hättig, “Pair natural orbitals in explicitly correlated second-order Møller–Plesset theory,” *Int. J. Quantum Chem.* **113**, 224–229 (2013), <https://onlinelibrary.wiley.com/doi/pdf/10.1002/qua.24098>.
- [77] G. Schmitz, C. Hättig, and D. P. Tew, “Explicitly correlated PNO-MP2 and PNO-CCSD and their application to the S66 set and large molecular systems”, *Phys. Chem. Chem. Phys.* **16**, 22167–22178 (2014).
- [78] Q. Ma and H.-J. Werner, “Scalable Electron Correlation Methods. 5. Parallel Perturbative Triples Correction for Explicitly Correlated Local Coupled Cluster with Pair Natural Orbitals,” *J. Chem. Theory Comput.* **14**, 198–215 (2018), PMID: 29211961, <https://doi.org/10.1021/acs.jctc.7b01141>.
- [79] F. Pavošević, P. Pinski, C. Riplinger, F. Neese, and E. F. Valeev, “SparseMaps—A systematic infrastructure for reduced-scaling electronic structure methods. IV. Linear-scaling second-order explicitly correlated energy with pair natural orbitals,” *J. Chem. Phys.* **144**, 144109 (2016).
- [80] F. Pavošević, C. Peng, P. Pinski, C. Riplinger, F. Neese, and E. F. Valeev, “SparseMaps—A systematic infrastructure for reduced scaling electronic structure methods. V. Linear scaling explicitly correlated coupled-cluster method with pair natural orbitals,” *J. Chem. Phys.* **146**, 174108 (2017).
- [81] E. F. Valeev and T. Daniel Crawford, “Simple coupled-cluster singles and doubles method with perturbative inclusion of triples and explicitly correlated geminals: The CCSD(T)R12 model,” *J. Chem. Phys.* **128**, 244113 (2008), <https://doi.org/10.1063/1.2939577>.
- [82] F. Neese, “The ORCA program system,” *WIREs Comput. Mol. Sci.* **2**, 73–78 (2011).
- [83] L. Kong, F. A. Bischoff, and E. F. Valeev, “Explicitly correlated R12/F12 methods for electronic structure.” *Chem. Rev.* **112**, 75–107 (2012).
- [84] T. Helgaker, P. Jørgensen, and J. Olsen, *Molecular Electronic-Structure Theory*, 1st ed. (John

- Wiley & Sons, Ltd, Chichester, UK, 2000).
- [85] J. F. Stanton, "Why CCSD (T) works: a different perspective," *Chem. Phys. Lett.* (1997).
- [86] A. G. Taube and R. J. Bartlett, "Improving upon CCSD(T): LambdaCCSD(T). I. Potential energy surfaces," *J. Chem. Phys.* **128**, 044110 (2008).
- [87] H. Fliegl, C. Hättig, and W. Klopper, "Inclusion of the (T) triples correction into the linear-r12 corrected coupled-cluster model CCSD(R12)," *International Journal of Quantum Chemistry* **106**, 2306–2317 (2006), <https://onlinelibrary.wiley.com/doi/pdf/10.1002/qua.20991>.
- [88] T. B. Adler, G. Knizia, and H.-J. Werner, "A simple and efficient ccsd(t)-f12 approximation," *J. Chem. Phys.* **127**, 221106 (2007), <https://doi.org/10.1063/1.2817618>.
- [89] D. P. Tew, W. Klopper, and C. Hättig, "A diagonal orbital-invariant explicitly-correlated coupled-cluster method," *Chem. Phys. Lett.* **452**, 326 – 332 (2008).
- [90] T. Shiozaki, M. Kamiya, S. Hirata, and E. F. Valeev, "Equations of explicitly-correlated coupled-cluster methods," *Phys. Chem. Chem. Phys.* **10**, 3358–3370 (2008).
- [91] C. Hättig, D. P. Tew, and A. Köhn, "Communications: Accurate and efficient approximations to explicitly correlated coupled-cluster singles and doubles, CCSD-F12," *J. Chem. Phys.* **132**, 231102–231102–4 (2010).
- [92] D. Kats and D. P. Tew, "Orbital-Optimized Distinguishable Cluster Theory with Explicit Correlation," *J. Chem. Theory Comput.* **15**, 13–17 (2019), <https://doi.org/10.1021/acs.jctc.8b01047>.
- [93] F. Pavošević, F. Neese, and E. F. Valeev, "Geminal-spanning orbitals make explicitly correlated reduced-scaling coupled-cluster methods robust, yet simple," *J. Chem. Phys.* **141**, 054106 (2014), <https://doi.org/10.1063/1.4890002>.
- [94] D. P. Tew and W. Klopper, "New correlation factors for explicitly correlated electronic wave functions," *J. Chem. Phys.* **123**, 074101 (2005), <https://doi.org/10.1063/1.1999632>.
- [95] A. J. May, E. Valeev, R. Polly, and F. R. Manby, "Analysis of the errors in explicitly correlated electronic structure theory," *Phys. Chem. Chem. Phys.* **7**, 2710–2713 (2005).
- [96] K. A. Peterson, T. B. Adler, and H.-J. Werner, "Systematically convergent basis sets for explicitly correlated wavefunctions: The atoms H, He, B–Ne, and Al–Ar," *J. Chem. Phys.* **128**, 084102 (2008), <https://doi.org/10.1063/1.2831537>.
- [97] M. Torheyden and E. F. Valeev, "Variational formulation of perturbative explicitly-correlated coupled-cluster methods," *Phys. Chem. Chem. Phys.* **10**, 3410–3420 (2008).

- [98] J. Foster and S. Boys, “Canonical Configurational Interaction Procedure,” *Rev. Mod. Phys.* **32**, 300–302 (1960).
- [99] K. G. Dyall, “The choice of a zeroth-order Hamiltonian for second-order perturbation theory with a complete active space self-consistent-field reference function,” *J. Chem. Phys.* **102**, 4909–4918 (1995), <https://doi.org/10.1063/1.469539>.
- [100] D. E. Woon and T. H. Dunning Jr., “Gaussian basis sets for use in correlated molecular calculations. III. The atoms aluminum through argon,” *J. Chem. Phys.* **98**, 1358–1371 (1993).
- [101] F. Weigend and R. Ahlrichs, “Balanced basis sets of split valence, triple zeta valence and quadruple zeta valence quality for H to Rn: Design and assessment of accuracy,” *Physical Chemistry Chemical Physics* **7**, 3297–3305 (2005).
- [102] F. Weigend, A. Köhn, and C. Hättig, “Efficient use of the correlation consistent basis sets in resolution of the identity MP2 calculations,” *J. Chem. Phys.* **116**, 3175–3183 (2002), <https://doi.org/10.1063/1.1445115>.
- [103] F. Weigend, “Accurate Coulomb-fitting basis sets for H to Rn,” *Physical Chemistry Chemical Physics* **8**, 1057–1065 (2006).
- [104] C. Hättig, “Optimization of auxiliary basis sets for RI-MP2 and RI-CC2 calculations: Core-valence and quintuple- ζ basis sets for H to Ar and QZVPP basis sets for Li to Kr,” *Phys. Chem. Chem. Phys.* **7**, 59 (2005).
- [105] K. E. Yousaf and K. A. Peterson, “Optimized auxiliary basis sets for explicitly correlated methods,” *J. Chem. Phys.* **129**, 184108 (2008), <https://doi.org/10.1063/1.3009271>.
- [106] R. Izsák and F. Neese, “An overlap fitted chain of spheres exchange method,” *J. Chem. Phys.* **135**, 144105 (2011), <https://doi.org/10.1063/1.3646921>.
- [107] S. J. Klippenstein, L. B. Harding, and B. Ruscic, “Ab Initio Computations and Active Thermochemical Tables Hand in Hand: Heats of Formation of Core Combustion Species,” *J. Phys. Chem. A* **121**, 6580–6602 (2017), pMID: 28758403, <https://doi.org/10.1021/acs.jpca.7b05945>.
- [108] G. Knizia, T. B. Adler, and H.-J. Werner, “Simplified CCSD(T)-F12 methods: Theory and benchmarks,” *J. Chem. Phys.* **130**, 054104 (2009).
- [109] M. C. Clement, J. Zhang, C. A. Lewis, C. Yang, and E. F. Valeev, “Optimized Pair Natural Orbitals for the Coupled Cluster Methods,” *J. Chem. Theory Comput.* **14**, 4581–4589 (2018).
- [110] H.-J. Werner, “Eliminating the domain error in local explicitly correlated second-order Møller–Plesset perturbation theory,” *J. Chem. Phys.* **129**, 101103 (2008),

- <https://doi.org/10.1063/1.2982419>.
- [111] The equation displayed in Ref[107] has a small sign-related typo: The sign before the group with $E(C_a O_b N_c H_d)$ should be positive instead of negative.
- [112] B. Ruscic, R. E. Pinzon, M. L. Morton, G. von Laszewski, S. J. Bittner, S. G. Nijsure, K. A. Amin, M. Minkoff, and A. F. Wagner, "Introduction to Active Thermochemical Tables: Several "Key" Enthalpies of Formation Revisited," *J. Phys. Chem. A* **108**, 9979–9997 (2004), <https://doi.org/10.1021/jp047912y>.
- [113] Y. Guo, C. Riplinger, U. Becker, D. G. Liakos, Y. Minenkov, L. Cavallo, and F. Neese, "Communication: An improved linear scaling perturbative triples correction for the domain based local pair-natural orbital based singles and doubles coupled cluster method [DLPNO-CCSD(T)]," *J. Chem. Phys.* **148**, 011101 (2018), <https://doi.org/10.1063/1.5011798>.
- [114] D. G. Liakos, Y. Guo, and F. Neese, "Comprehensive Benchmark Results for the Domain Based Local Pair Natural Orbital Coupled Cluster Method (DLPNO-CCSD(T)) for Closed- and Open-Shell Systems," *J. Phys. Chem. A* **124**, 90–100 (2019).
- [115] T. Helgaker, W. Klopper, H. Koch, and J. Noga, "Basis-set convergence of correlated calculations on water," *The Journal of Chemical Physics* **106**, 9639–9646 (1997), <https://doi.org/10.1063/1.473863>.
- [116] S. Ye, C. Riplinger, A. Hansen, C. Krebs, J. M. Bollinger Jr., and F. Neese, "Electronic Structure Analysis of the Oxygen-Activation Mechanism by FeII- and α -Ketoglutarate (α KG)-Dependent Dioxygenases," *Chem. Eur. J.* **18**, 6555–6567 (2012), <https://chemistry-europe.onlinelibrary.wiley.com/doi/pdf/10.1002/chem.201102829>.
- [117] T. Krämer, M. Kampa, W. Lubitz, M. van Gastel, and F. Neese, "Theoretical Spectroscopy of the NiII Intermediate States in the Catalytic Cycle and the Activation of [NiFe] Hydrogenases," *ChemBioChem* **14**, 1898–1905 (2013), <https://chemistry-europe.onlinelibrary.wiley.com/doi/pdf/10.1002/cbic.201300104>.
- [118] F. Müh and A. Zouni, "The nonheme iron in photosystem II," *Photosynth. Res.* **116**, 295–314 (2013).
- [119] T. Yanai, D. P. Tew, and N. C. Handy, "A new hybrid exchange–correlation functional using the Coulomb-attenuating method (CAM-B3LYP)," *Chem. Phys. Lett.* **393**, 51 – 57 (2004).
- [120] {def2-TZVP, def2-TZVP/RI, cc-pVDZ-F12-OptRI}, TightPNO.
- [121] {def2-SVP, def2-SVP/RI, *uncontracted* def2-TZVPP}, NormalPNO.

- [122] {def2-TZVPP, def2-TZVPP/RI, *uncontracted* def2-QZVPP}, NormalPNO.
- [123] CABS space includes AOs as well in CABS+ approach.
- [124] J. C. Slater, “The Normal State of Helium,” *Phys. Rev.* **32**, 349–360 (1928).
- [125] E. A. Hylleraas, “Neue Berechnung der Energie des Heliums im Grundzustande, sowie des tiefsten Terms von Ortho-Helium,” *Zeitschrift für Physik* **54**, 347–366 (1929).
- [126] E. A. Hylleraas, “Über den Grundterm der Zweielektronenprobleme von H-, He, Li+, Be++ usw.” *Zeitschrift für Physik* **65**, 209—225 (1930).
- [127] J. W. Boughton and P. Pulay, “Comparison of the Boys and Pipek-Mezey localizations in the local correlation approach and automatic virtual basis selection,” *J. Comput. Chem.* **14**, 736–740 (1993).
- [128] A. Köhn, G. W. Richings, and D. P. Tew, “Implementation of the full explicitly correlated coupled-cluster singles and doubles model CCSD-F12 with optimally reduced auxiliary basis dependence,” *J. Chem. Phys.* **129**, 201103 (2008).
- [129] S. Ten-no and J. Noga, “Explicitly correlated electronic structure theory from R12/F12 ansätze,” *WIREs Comput. Mol. Sci.* **2**, 114–125 (2012).